AFRL-OSR-VA-TR-2015-0127

Dynamic Data Driven Methods for Self-aware Aerospace Vehicles

Karen Willcox
MASSACHUSETTS INSTITUTE OF TECHNOLOGY

04/08/2015
Final Report

Air Force Research Laboratory
AF Office Of Scientific Research (AFOSR)/ RTC
Arlington, Virginia 22203
Air Force Materiel Command

REPORT DOCUMENTATION PAGE

Form Approved
OMB No. 0704-0188

1. REPORT DATE *(DD-MM-YYYY)*	**2. REPORT TYPE**	**3. DATES COVERED** *(From - To)*
04/01/2015	Final	9/30/11-1/31/15

4. TITLE AND SUBTITLE
Dynamic Data Driven Methods for Self-aware Aerospace Vehicles

5a. CONTRACT NUMBER

5b. GRANT NUMBER
FA9550-11-1-0339

5c. PROGRAM ELEMENT NUMBER

6. AUTHOR(S)
Karen E. Willcox
Douglas Allaire
George Biros
Jeffrey Chambers
Omar Ghattas
David Kordonowy

5d. PROJECT NUMBER

5e. TASK NUMBER

5f. WORK UNIT NUMBER

7. PERFORMING ORGANIZATION NAME(S) AND ADDRESS(ES)
Massachusetts Institute of Technology
77 Massachusetts Avenue
Cambridge, MA 02139

8. PERFORMING ORGANIZATION REPORT NUMBER

9. SPONSORING/MONITORING AGENCY NAME(S) AND ADDRESS(ES)
Air Force Office of Scientific Research
875 N. Randolph St.
Arlington, VA 22203

10. SPONSOR/MONITOR'S ACRONYM(S)

11. SPONSOR/MONITOR'S REPORT NUMBER(S)

12. DISTRIBUTION/AVAILABILITY STATEMENT
Approved for Public Release

13. SUPPLEMENTARY NOTES

14. ABSTRACT
This project aimed to develop novel inference approaches for dynamic vehicle state estimation and methods for online management of multifidelity models and sensor data, and to apply the new methods to quantify the benefits of a self-aware unmanned aerial vehicle (UAV) in terms of reliability, maneuverability and survivability. The project accomplished all objectives and resulted in the development of new DDDAS methodology and DDDAS algorithms, new models for a DDDAS-enabled self-aware UAV, and a demonstration of the value of DDDAS in the context of dynamic data-driven structural assessment to support decision-making for a damaged vehicle taking evasive action in a hostile environment.

15. SUBJECT TERMS
Dynamic data driven application systems (DDDAS); surrogate modeling; reduced order modeling; multifidelity methods; self-aware UAV.

16. SECURITY CLASSIFICATION OF:			**17. LIMITATION OF ABSTRACT**	**18. NUMBER OF PAGES**	**19a. NAME OF RESPONSIBLE PERSON**
a. REPORT	**b. ABSTRACT**	**c. THIS PAGE**			Karen Willcox
U	U	U		37	**19b. TELEPHONE NUMBER** *(Include area code)* 617-253-3503

INSTRUCTIONS FOR COMPLETING SF 298

1. REPORT DATE. Full publication date, including day, month, if available. Must cite at least the year and be Year 2000 compliant, e.g. 30-06-1998; xx-06-1998; xx-xx-1998.

2. REPORT TYPE. State the type of report, such as final, technical, interim, memorandum, master's thesis, progress, quarterly, research, special, group study, etc.

3. DATE COVERED. Indicate the time during which the work was performed and the report was written, e.g., Jun 1997 - Jun 1998; 1-10 Jun 1996; May - Nov 1998; Nov 1998.

4. TITLE. Enter title and subtitle with volume number and part number, if applicable. On classified documents, enter the title classification in parentheses.

5a. CONTRACT NUMBER. Enter all contract numbers as they appear in the report, e.g. F33315-86-C-5169.

5b. GRANT NUMBER. Enter all grant numbers as they appear in the report. e.g. AFOSR-82-1234.

5c. PROGRAM ELEMENT NUMBER. Enter all program element numbers as they appear in the report, e.g. 61101A.

5e. TASK NUMBER. Enter all task numbers as they appear in the report, e.g. 05; RF0330201; T4112.

5f. WORK UNIT NUMBER. Enter all work unit numbers as they appear in the report, e.g. 001; AFAPL30480105.

6. AUTHOR(S). Enter name(s) of person(s) responsible for writing the report, performing the research, or credited with the content of the report. The form of entry is the last name, first name, middle initial, and additional qualifiers separated by commas, e.g. Smith, Richard, J, Jr.

7. PERFORMING ORGANIZATION NAME(S) AND ADDRESS(ES). Self-explanatory.

8. PERFORMING ORGANIZATION REPORT NUMBER. Enter all unique alphanumeric report numbers assigned by the performing organization, e.g. BRL-1234; AFWL-TR-85-4017-Vol-21-PT-2.

9. SPONSORING/MONITORING AGENCY NAME(S) AND ADDRESS(ES). Enter the name and address of the organization(s) financially responsible for and monitoring the work.

10. SPONSOR/MONITOR'S ACRONYM(S). Enter, if available, e.g. BRL, ARDEC, NADC.

11. SPONSOR/MONITOR'S REPORT NUMBER(S). Enter report number as assigned by the sponsoring/ monitoring agency, if available, e.g. BRL-TR-829; -215.

12. DISTRIBUTION/AVAILABILITY STATEMENT. Use agency-mandated availability statements to indicate the public availability or distribution limitations of the report. If additional limitations/ restrictions or special markings are indicated, follow agency authorization procedures, e.g. RD/FRD, PROPIN, ITAR, etc. Include copyright information.

13. SUPPLEMENTARY NOTES. Enter information not included elsewhere such as: prepared in cooperation with; translation of; report supersedes; old edition number, etc.

14. ABSTRACT. A brief (approximately 200 words) factual summary of the most significant information.

15. SUBJECT TERMS. Key words or phrases identifying major concepts in the report.

16. SECURITY CLASSIFICATION. Enter security classification in accordance with security classification regulations, e.g. U, C, S, etc. If this form contains classified information, stamp classification level on the top and bottom of this page.

17. LIMITATION OF ABSTRACT. This block must be completed to assign a distribution limitation to the abstract. Enter UU (Unclassified Unlimited) or SAR (Same as Report). An entry in this block is necessary if the abstract is to be limited.

Dynamic Data Driven Methods for Self-aware Aerospace Vehicles
Grant # FA9550-11-1-0339

Final Report

Participating Institutions: Aurora Flight Sciences, Massachusetts Institute of Technology, University of Texas at Austin

Lead PI: Karen Willcox, Massachusetts Institute of Technology

Reporting Period: September 30, 2011 to January 31, 2015

Program Manager: Dr. Frederica Darema

Abstract

This project aimed to develop novel computational statistical inference approaches for dynamic vehicle state estimation through a combination of machine learning and reduced-order modeling techniques, to develop adaptive model reduction approaches that use dynamic data to update reduced-order models for vehicle flight limit prediction, to develop approaches for online management of multifidelity models and sensor data, and to apply the new methods to quantify the benefits of a self-aware unmanned aerial vehicle (UAV) in terms of reliability, maneuverability and survivability. The project accomplished all objectives and resulted in the development of new DDDAS methodology and DDDAS algorithms, new models for a DDDAS-enabled self-aware UAV, and a demonstration of the value of DDDAS in the context of dynamic data-driven structural assessment to support decision-making for a damaged vehicle taking evasive action in a hostile environment.

Contents

1 Project objectives

The specific research objectives of this research were proposed as:

1. To develop novel computational statistical inference approaches for dynamic vehicle state estimation, through a combination of machine learning and reduced-order modeling techniques.

2. To develop adaptive model reduction approaches that use dynamic data to update reduced-order models for vehicle flight limit prediction.

3. To develop approaches for online management of multifidelity models and sensor data, using variance-based sensitivity analysis.

4. To apply our new methods to quantify the benefits of a self-aware UAV in terms of reliability, maneuverability and survivability.

The project has accomplished all these objectives. Objective 3 was achieved using support vector machines and self-organizing maps, rather than variance-based sensitivity analysis. The remainder of this report summarizes the main project outcomes and accomplishments.

2 Project Outcomes and Accomplishments

2.1 Summary

The project has resulted in the development of new DDDAS methodology and DDDAS algorithms, new models for a DDDAS-enabled self-aware unmanned aerial vehicle (UAV), and a demonstration of the value of DDDAS in the context of dynamic data-driven structural assessment to support decision-making for a damaged vehicle taking evasive action in a hostile environment. The specific project accomplishments include the following:

- **A conceptual design framework for a DDDAS-enabled UAV.** The framework includes sizing of the UAV at the overall vehicle level and detailed finite element analysis at the panel level. It also includes a structural response model that incorporates multiple degradation or failure modes including damaged panel strength (BVID, thru-hole), damaged panel stiffness (BVID, thru-hole), loose fastener, fretted fastener hole, and disbonded surface.

- **A new data-driven approach for the online updating of the flight envelope of a DDDAS-enabled self-aware UAV subjected to structural degradation.** The main contribution of this part of the work is a general methodology that leverages both physics-based modeling and data to decompose tasks into two phases: expensive offline simulations to build an efficient characterization of the problem, and rapid data-driven classification to support online decision-making. In the approach, physics-based models at the wing and vehicle level run offline to generate libraries of information covering a range of damage scenarios. These libraries are queried online to estimate vehicle capability states. The state estimation and associated quantification of uncertainty are achieved by Bayesian classification using sensed strain data.

- **A demonstration of the value of DDDAS on a conceptual UAV executing a pull-up maneuver, where the vehicle flight envelope is updated dynamically with onboard sensor information.** During vehicle operation, the maximum maneuvering load factor is

estimated using structural strain sensor measurements combined with physics-based information from pre-computed damage scenarios that consider structural weakness. Compared to a baseline case that uses a static as-designed flight envelope, the self-aware vehicle achieves both an increase in probability of executing a successful maneuver and an increase in overall usage of the vehicle capability.

- **A new data-driven strategy for online structural assessment at the panel level for a DDDAS-enabled self-aware UAV.** During the offline phase, high-fidelity finite element simulations are used to construct reduced-order models and classification criteria: proper orthogonal decomposition approximations and self-organizing maps are combined to realize a fast mapping from measured quantities to system capabilities. During the online phase, the surrogate mapping is employed to directly estimate the vehicle's evolving structural capability from sensor data. The approach has been demonstrated for a test problem of a composite wing panel on an unmanned aerial vehicle that undergoes degradation in structural properties.

- **A new algorithm for fast kernel density estimation in high dimensions.** We introduced novel methods for pruning and approximating the far field. Our far field approximation requires only kernel evaluations and does not use analytic expansions. Pruning is not done using bounding boxes but rather combinatorially using a sparsified nearest-neighbor graph of the input. The time complexity of our algorithm depends linearly on the ambient dimension. The error in the algorithm depends on the low-rank approximability of the far field, which in turn depends on the kernel function and on the intrinsic dimensionality of the distribution of the points. The error of the far field approximation does not depend on the ambient dimension. We report results for Gaussian kernel sums for 100 million points in 64 dimensions, for one million points in 1000 dimensions, and for problems in which the Gaussian kernel has a variable bandwidth. To the best of our knowledge, all of these experiments are impossible or prohibitively expensive with existing fast kernel summation methods.

- **Fast algorithms for Bayesian inverse medium problems.** We consider a supervised inverse medium problem algorithm using a Bayesian framework and a variational formulation for a maximum a posteriori (MAP) estimation of the label field. In the Bayesian framework, we must define the likelihood function (the probability of the data given the label field) and the prior probability (for the label field). We propose a non-parametric, high-dimensional, kernel density estimation (KDE) for the likelihood function, based on Gabor features (300 per pixel). This approach better approximates non-local correlations. For the prior function, we use a simple smoothness prior. We provide experimental evidence that this likelihood function performs very well and converges to the correct segmentation with the number of training datasets.

These accomplishments are described in more detail in the following sections.

2.2 Aircraft Design

A conceptual design of a UAV was established to allow for the assessment of structural damage and degradation cases on realistic maneuvers from a vehicle. The design was completed using first-principles sizing and Federal Aviation Regulation (FAR) 23 guidelines (similar to NASA CR-2010-216794/VOL2 and AFOSR Final Report for contract FA9550-10-C-0175). Aurora utilized an internally developed Bayesian Multi-Disciplinary Optimization (BMDO) code to generate the conceptual design. The vehicle has a wing span of 55 feet, a cruise speed of 140 knots at an altitude

of 25,000 feet, and a 500 pound payload capability. The range of the aircraft is estimated to be roughly 2500 nautical miles, corresponding to a duration of 17.5 hours. An illustration of the vehicle is shown in Figure 1. The estimated weights of the component comprising the conceptual

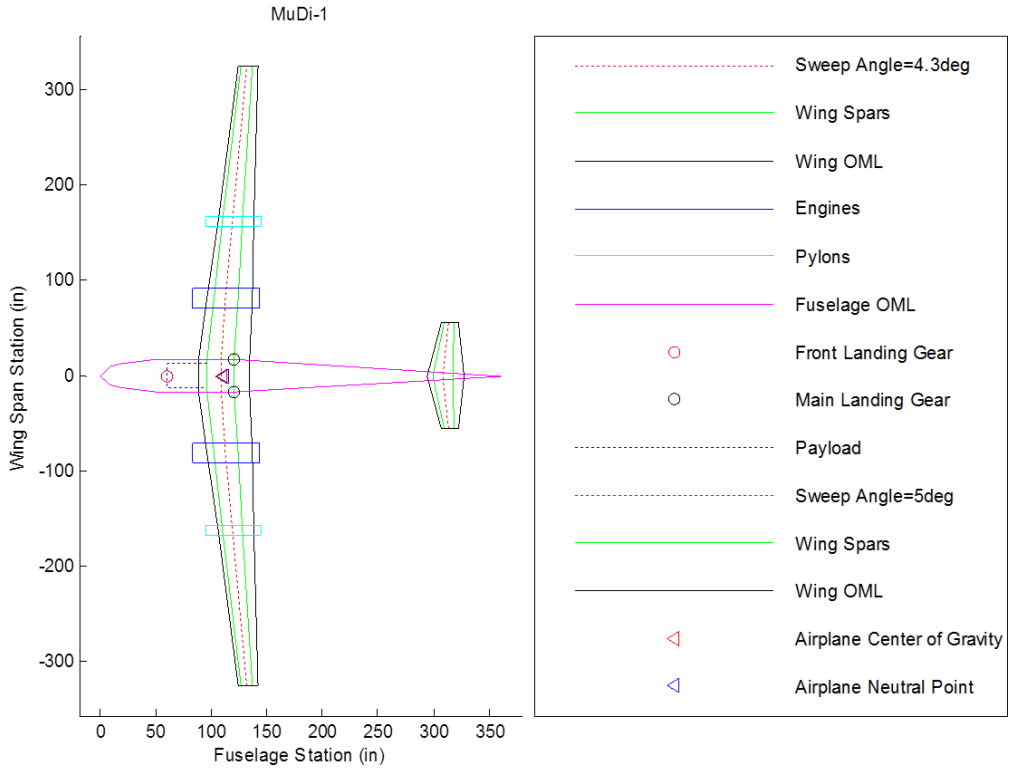

Figure 1: Conceptual aircraft design.

design are included in Table 1 and the relative percentage of each component is shown in Figure 2. Characteristic speeds of the conceptual UAV are included in Table 2 and characteristics of the lifting surfaces of the vehicle are included in Table 3. The design of this conceptual UAV allows for adequate range and duration to explore capability as a function of the changing structural state of the vehicle.

The aerodynamic characteristics of the wings are determined using the low Reynolds number airfoil design and analysis code, XFOIL. XFOIL is an interactive program for the design and analysis of subsonic isolated airfoils. The Reynolds number, Re, is a dimensionless number that gives a measure of the ratio of inertial forces to viscous forces:

$$Re = \frac{vL}{\nu} \tag{1}$$

where v is the mean velocity of the aircraft, L is a characteristic linear dimension, and ν is the kinematic viscosity. Reynolds numbers are use in airfoil design to manage "scale effect" when computing/comparing characteristics. For this work, the mean velocity is taken as the flight speed, V, the characteristic length is the average chord length, c, and the kinematic viscosity of the air is taken at cruise altitude:

$$Re = \frac{Vc}{2.126 \times 10^{-5} \frac{m^2}{s}} \tag{2}$$

$$Re = \frac{\left(72.0 \frac{m}{s}\right)(1.614m)}{2.126 \times 10^{-5} \frac{m^2}{s}} = 5.47 \times 10^6 \tag{3}$$

Table 1: Component weights of the conceptual UAV

Component	Weight (lbs.)
Fuselage	476.2
Wing	286.6
Payload	500.0
Vertical Tail	22.4
Horz. Tail	7.5
Engine	423.5
Pylon	25.0
Fuel	1060.8
HPE System	225.0
Nose LG	31.4
Main LG	174.1
Sum	**3232.5**

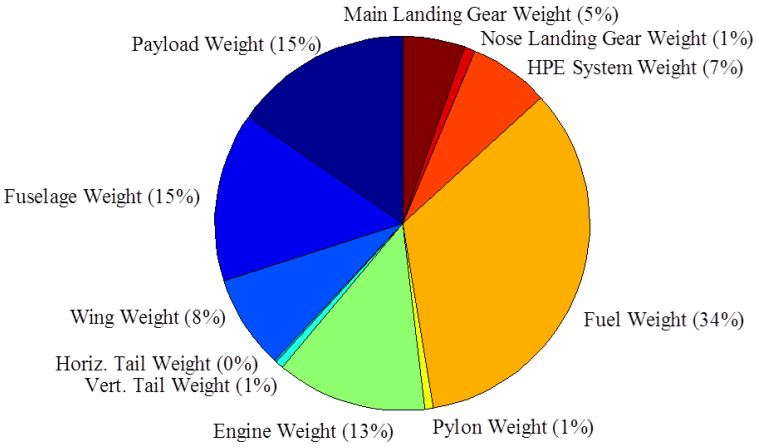

Figure 2: Pie chart of the estimated weights of the components comprising the conceptual UAV design.

Results from the XFOIL analysis are displayed in Figures 3 and 4, the lift coefficient versus the angle of attack and drag coefficient, respectively. In order to approximate the lift at cruise, the wing lift coefficient, C_L, is assumed equal to the airfoil lift coefficient, C_l:

$$W = L = qSC_L \cong qSC_l \tag{4}$$

where the airfoil coefficient is calculated for 140 KTAS at 15000 feet to be:

$$C_l = \frac{1}{q}\left(\frac{W}{S}\right) = \frac{1}{41.6\frac{lbs}{ft^2}}\left(\frac{3232.5lbs}{146.7ft^2}\right) = 0.5291 \tag{5}$$

The resulting wing incidence required for level fuselage during cruise is $0.885°$. The plots of C_L and C_L/C_D versus the angle of attack are shown in Figure 5. The maximum lift coefficient (clean) depends on the airfoil characteristics. The following equations are valid for high-aspect-ratio wings with moderate sweep:

$$L_{max} = qSC_{L_{max}} \tag{6}$$

Table 2: Characteristic speeds of the conceptual UAV

Aircraft Speed	Speed [KTAS]	Speed [m/s]
V_A	66.9	34.4
V_S	57.5	29.6
V_C (cruise and loiter)	140.0	72.0
V_D	168.0	86.4

Table 3: Characteristic of the conceptual UAV

Metric	Variable	Value	
Takeoff Weight	W	3257.3	lbs
Wing Area	S	146.7	in^2
Wing Sweep	Λ	4.3	$^\circ$
Wing Span	b	54.2	ft
Wing Root Chord	c_o	3.79	ft
Wing Tip Chord	c_t	1.52	ft
Wing Aspect Ratio	AR	20	
Front Spar Location	ξ_{fspar}	15	%
Rear Spar Location	ξ_{rspar}	70	%
Wing Airfoil		DA01	
Horz. Tail Airfoil		NACA 0012	
Vert. Tail Airfoil		NAVA 0012	

$$C_{L_{max}} = 0.9 C_{l_{max}} \cos \Lambda_{\frac{c}{4}} = 0.9\,(1.8263) \cos\,(4.3^\circ) = 1.64 \tag{7}$$

$$L_{max} = \left(41.6\ \frac{\text{lbs}}{\text{ft}^2}\right)\left(146.7\ \text{ft}^2\right)(1.64) = 10002\ \text{lbs} \tag{8}$$

$$n_{max} = \frac{L_{max}}{W} = \frac{10002\ \text{lbs}}{3232.5\ \text{lbs}} = 3.09 \tag{9}$$

This load factor is less than 3.8, which would correspond to a $C_{L_{max}}$ of 2.01. Note, these calculations do not account for control surfaces. A plot from Raymer's *Aircraft Design: A Conceptual Approach* [11] provides maximum-lift trends versus sweep angle for several classes of aircraft, shown in Figure 6. From the wing loading and maximum lift coefficient, the stall speed of the aircraft can be determined:

$$W = L = q_{stall} S C_{L_{max}} \tag{10}$$

$$V_{stall} = \sqrt{\frac{2}{\rho}\left(\frac{W}{S}\right)\frac{1}{C_{L_{max}}}} \tag{11}$$

where the clean wing stall speed at various altitudes is:

$$q_{stall} = \left(\frac{W}{S}\right)\frac{1}{C_{L_{max}}} = \left(\frac{3232.5\ \text{lbs}}{146.7\ \text{ft}^2}\right)\frac{1}{1.64} = 13.4\frac{\text{lbs}}{\text{ft}^2} \tag{12}$$

Therefore, the stall velocity is:

$$V_{stall} = \sqrt{\frac{2 q_{stall}}{\rho}} \tag{13}$$

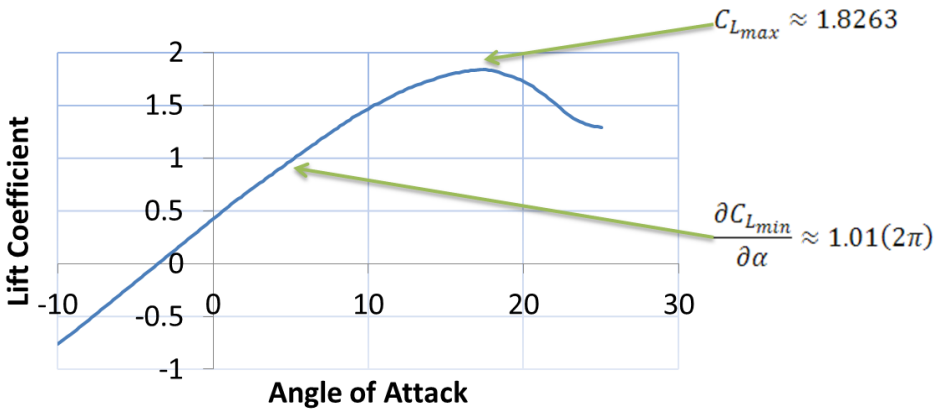

Figure 3: Lift coefficient versus angle of attack for $Re = 5.47 \times 10^6$.

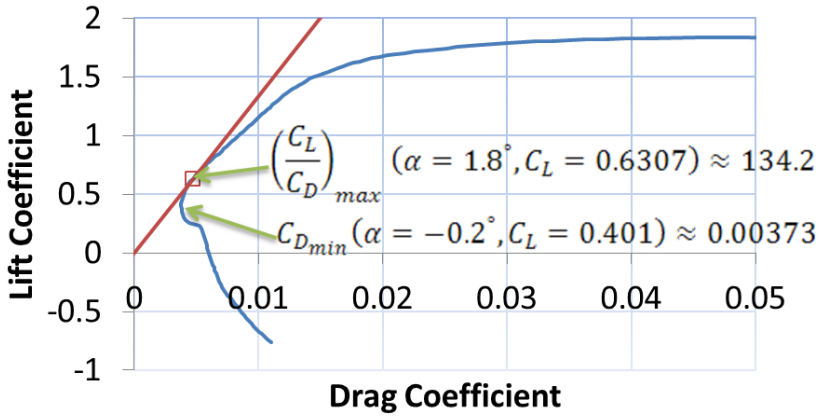

Figure 4: Lift coefficient versus drag coefficient for $Re = 5.47 \times 10^6$.

The stall velocity at three different altitudes of interest can be calculated:

$$V_{stall}\,(h = 0ft) = 106.3\frac{\text{ft}}{\text{s}} = 63.0 \text{ knots} \tag{14}$$

$$V_{stall}\,(h = 15000ft) = 134.3\frac{\text{ft}}{\text{s}} = 79.6 \text{ knots} \tag{15}$$

$$V_{stall}\,(h = 25000ft) = 159.3\frac{\text{ft}}{\text{s}} = 94.4 \text{ knots} \tag{16}$$

The stall speed at 15000 feet, Equation 15, is below the designed 140 knots (72.0 m/s) cruise speed, as indicated in Table 2. This means that the wing will not stall at cruise, but the stall speed is less than the desired 57.5 knots stall speed. The lack of control surfaces increases stall speed:

$$V_{stall} = \sqrt{\frac{2}{\rho}\left(\frac{W}{S}\right)\frac{1}{C_{L_{max}}}} \propto \sqrt{\frac{1}{C_{L_{max}}}} \tag{17}$$

Mandatory separation from stall speed, as specified in FAR 23, pushes the minimum maneuver speed above the design point:

$$V_{A_{min}} = V_S\sqrt{n} \tag{18}$$

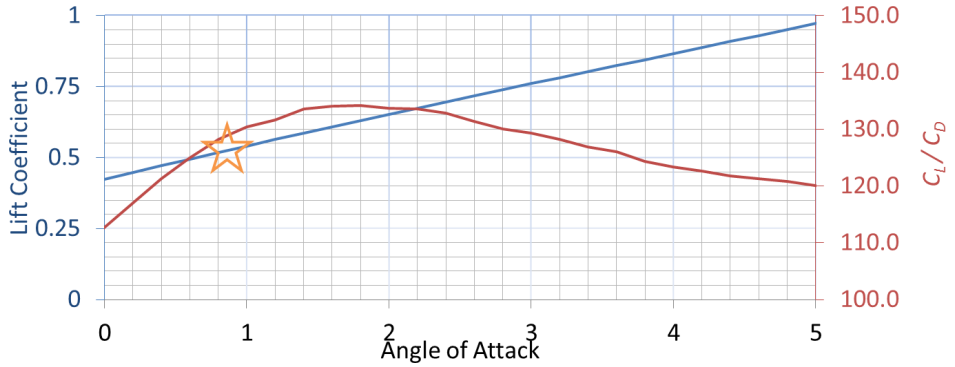

Figure 5: Lift coefficient and lift coefficient divided by drag coefficient versus angle of attack.

$$V_{C_{min}} = min\left(33\sqrt{\frac{W}{S}}, V_{A_{min}}\right) \tag{19}$$

$$V_{D_{min}} = 1.40 V_{C_{min}} \tag{20}$$

Table 4 contains the minimum speeds for the three altitudes.

Table 4: Minimum maneuver speeds, as mandated in FAR 23, for the conceptual design

Aircraft Speed	Speed								
	Altitude = 0 ft			Altitude = 15000 ft			Altitude = 25000 ft		
	KEAS	KTAS	m/s	KEAS	KTAS	m/s	KEAS	KTAS	m/s
$V_{A_{min}}$	122.8	122.8	63.2	155.1	195.8	100.8	183.9	275.6	141.8
$V_{S_{min}}$	63.0	63.0	32.4	79.6	100.5	51.7	94.4	141.4	72.7
$V_{C_{min}}$	154.4	154.4	79.4	155.1	195.8	100.8	184.0	275.6	141.8
$V_{D_{min}}$	215.9	215.9	111.1	216.9	273.9	140.9	257.3	385.4	198.3

For initial assessment of the DDDAS algorithms, the aircraft performs a standard rate turn. A sustained standard rate turn is performed by banking the aircraft at an angle, α, and increasing the lift normal to the wing planform. Increasing the lift is necessary to balance the aircraft weight while creating a net centripetal force perpendicular to the velocity, V, of the aircraft. The constant turn radius, r, is equal to the velocity, V, divided by the turn rate, $\dot{\psi}$:

$$r = \frac{V}{\dot{\psi}} \tag{21}$$

The turn rate, $\dot{\psi}$, is calculated as:

$$\dot{\psi} = \frac{g\sqrt{n^2 - 1}}{V} \tag{22}$$

where g is the acceleration of gravity, n is the load factor (ratio of lift of the aircraft to its weight), and V is the velocity. The variables involved with the standard turn are illustrated in Figure 7. Equation 22 can be rearranged to give the load factor as a function of aircraft velocity and turn rate:

$$n = \sqrt{\left(\frac{\dot{\psi}V}{g}\right)^2 + 1} \tag{23}$$

Performing a standard rate turn allows the aircraft to change its heading at a constant velocity; a larger bank angle allows for a higher rotational speed and a tighter radius of turn, while increasing

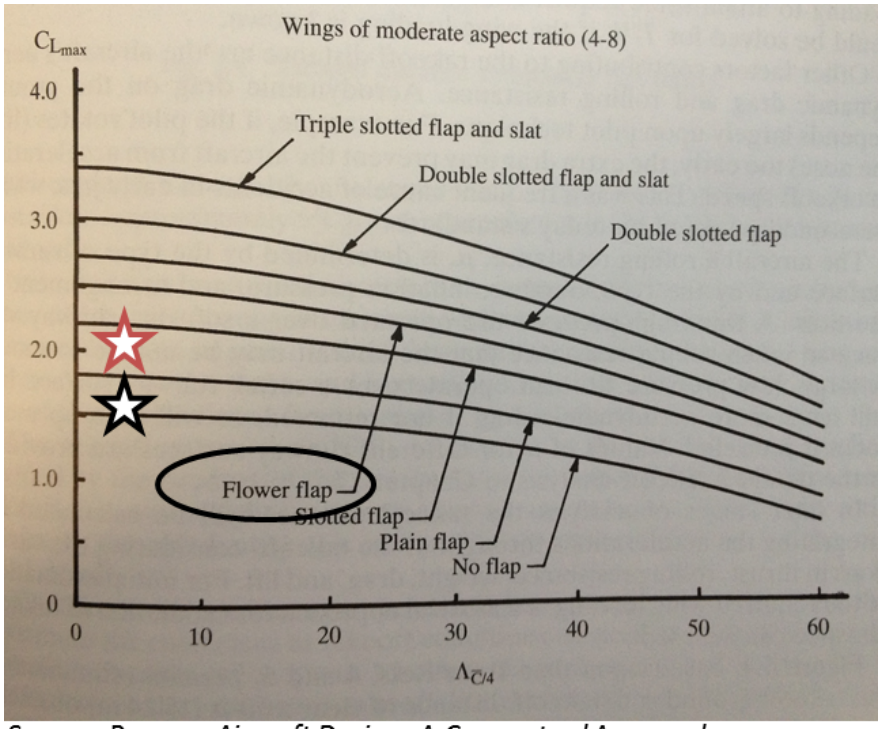

Source: Raymer *Aircraft Design: A Conceptual Approach*

Figure 6: Maximum lift coefficient versus angle of attack [11].

the lift force necessary to keep the aircraft at altitude. Increasing the load factor increases the loading on the structure of the aircraft.

The lift distribution along the wing for multiple turn rates and multiple radii is estimated using Schrenk's approximation based on an elliptical and chord-wise estimation of lift. This lift distribution is reacted by the wing box structure of the concept UAV in bending and shear. The cross-section of an example wing box is shown in Figure 8. The wing spar caps react the majority of bending while the wing spar webs react the majority of shear. These load reactions induce tension and compression stress in the lower and upper wing skins, respectively, due to bending; shear stress is induced in the spar web due to the shear loading. The basic relations for calculating the shear stress in the web and the tensile or compressive stress in the cap are given in Equations 24 and 25.

$$\tau_{web} = \frac{\mathcal{S}_{\perp(\eta)}}{A_{web(\eta)}} = \frac{\mathcal{S}_{\perp(\eta)}}{c_{\perp}^{2}\left(\eta\right)\bar{t}_{web_s}\left(\bar{h}_{fspar} + \bar{h}_{rspar}\right)} \tag{24}$$

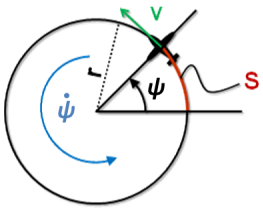

Figure 7: Standard rate turn variables.

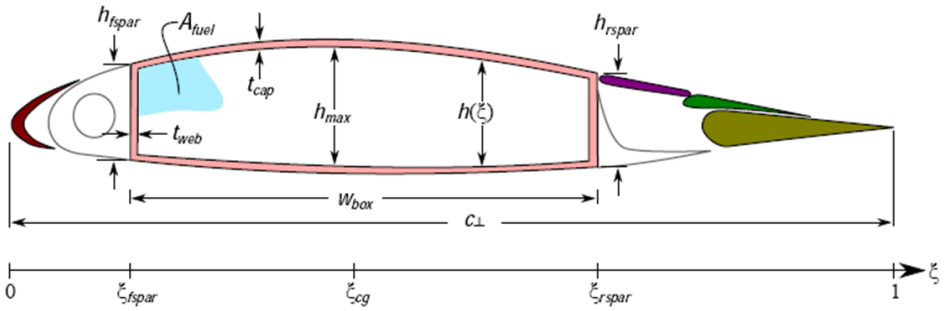

Figure 8: Cross-section of an example wing box.

$$\sigma_{cap} = \frac{\mathcal{M}_\perp(\eta)\, h_{max}}{2\left(I_{cap} + r_E I_{web}\right)} \simeq \frac{\mathcal{M}_\perp(\eta)\, \bar{h}_{max}}{2c_\perp^3(\eta)\, \bar{I}_{cap}} \tag{25}$$

These relations allow for estimating the turn rate or radius of the concept UAV based on the capability of the structural components to react the loading. As shown in Figure 8, a constant-percent chord control surfaces can be placed in front of or behind the wing box. Trailing edge flaps can occupy the last 30% of the chord and increase the lift coefficient and increase the wing area (Fowler-type extending flaps). The increase in lift coefficient is:

$$\Delta C_{l_{max}} = 1.9\frac{C'}{C} \tag{26}$$

Leading edge slats can occupy the first 15% of the chord and prevent premature airflow separation caused by the flap.

$$\Delta C_{l_{max}} = 0.4\frac{C'}{C} \tag{27}$$

Further investigating the increase in the coefficient of lift due to the addition of flaps, the change in the lift coefficient can be calculated via Equation 28:

$$\Delta C_{L_{max}} = 0.9\Delta C_{l_{max}} \left(\frac{S_{flapped}}{S_{ref}}\right) cos\Lambda_{H.L.} \tag{28}$$

Estimation of the maximum increase in lift coefficient, assume the control surfaces run the entire span, as shown in Figure 9 of the wing and that the leading edge extends the chord by 5%:

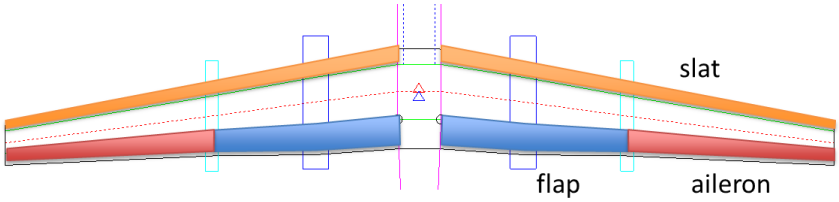

Figure 9: Spanwise location of control surfaces.

$$\Delta C_{L_{max}} = 0.9(0.4)(1.05)cos(6.4^\circ) = 0.38 \tag{29}$$

and assume the trailing edge extends the chord by 10%:

$$\Delta C_{L_{max}} = 0.9(1.9)(1.1)cos(3.1^\circ) = 1.87 \tag{30}$$

The total maximum lift coefficient becomes 3.89 (1.64 + 0.38 + 1.87).

The maximum lift and stall speed should now be revisited. Recalculating the maximum lift and load factor:

$$L_{max} = \left(41.6 \frac{\text{lbs}}{\text{ft}^2}\right)\left(146.7 \text{ ft}^2\right)(3.89) = 23740\text{lbs} \tag{31}$$

$$n_{max} = \frac{L_{max}}{W} = \frac{23740 \text{ lbs}}{3232.5 \text{ lbs}} = 7.34 \tag{32}$$

Recalculating the stall speeds:

$$q_{stall} = \left(\frac{W}{S}\right)\frac{1}{C_{L_{max}}} = \left(\frac{3232.5 \text{ lbs}}{146.7 \text{ ft}^2}\right)\frac{1}{3.89} = 5.66\frac{\text{lbs}}{\text{ft}^2} \tag{33}$$

$$V_{stall}\left(h = 0ft\right) = 69.0\frac{ft}{s} = 40.9knots \tag{34}$$

$$V_{stall}\left(h = 15000ft\right) = 87.2\frac{ft}{s} = 51.6knots \tag{35}$$

$$V_{stall}\left(h = 25000ft\right) = 103.4\frac{ft}{s} = 61.3knots \tag{36}$$

From the updated stall speeds, V-n diagrams are created for the three altitudes. These V-n diagrams are shown in Figures 10 through 12. The updated minimum speeds at the three altitudes are

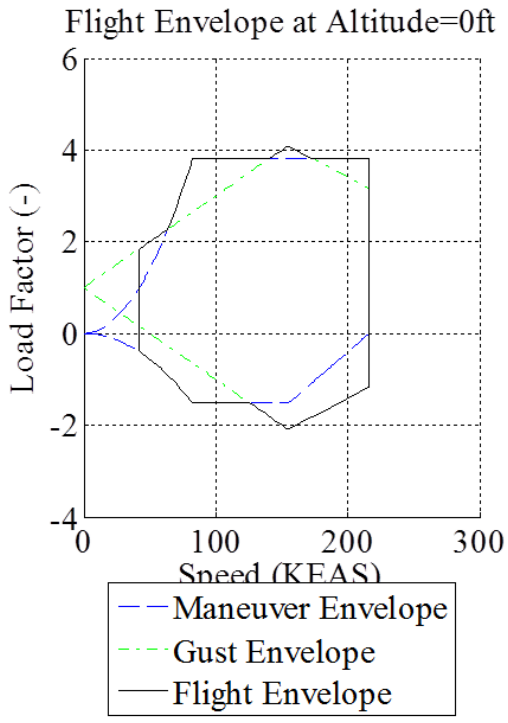

Figure 10: Flight envelope at an altitude of 0 feet.

updated in Table 5. $V_{A_{min}}$ is less than the designed 140 knots cruise speed. Therefore, the aircraft is able to maneuver at speeds of 140 knots (KTAS) at 15000 feet (minimum maneuver speed is 127.1 knots). While the cruise speed of the initially designed UAV was too low to meet FAR 23 due to wing loading, the necessary lift coefficient at 15000 feet was reduced by 50%. The viable design is therefore used in moving forward with the example problem.

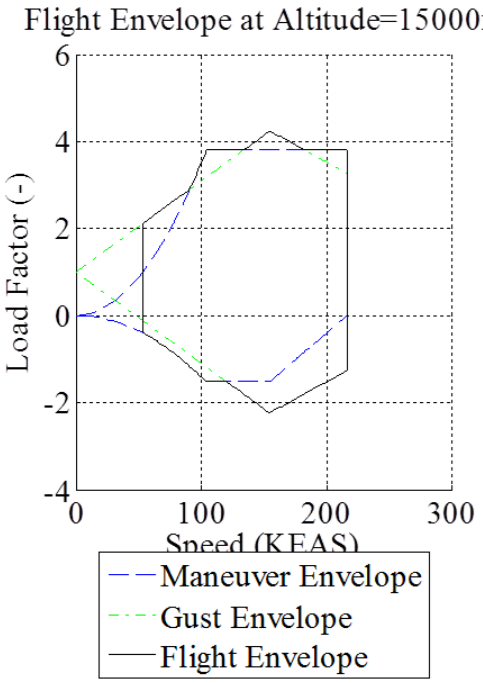

Figure 11: Flight envelope at an altitude of 15000 feet.

Table 5: Minimum maneuver speeds, as mandated in FAR 23, for the conceptual design with flaps

Aircraft Speed	Speed								
	Altitude = 0 ft			Altitude = 15000 ft			Altitude = 25000 ft		
	KEAS	KTAS	m/s	KEAS	KTAS	m/s	KEAS	KTAS	m/s
$V_{A_{min}}$	79.7	79.7	41.0	100.7	127.1	65.4	119.4	178.8	92.0
$V_{S_{min}}$	40.9	40.9	21.0	51.6	65.2	33.5	61.3	91.8	47.2
$V_{C_{min}}$	154.4	154.4	79.4	154.4	194.9	100.3	154.4	231.3	119.0
$V_{D_{min}}$	215.9	215.9	111.1	215.9	272.7	140.3	215.9	323.5	164.4

2.3 Finite Element Modeling

The magnitude of wing loading on the concept UAV is directly related to the turn rate; therefore a section of the wing is used as an example panel on which to test the algorithms developed under the DDDAS program. This allows for damage or degradation that reduces the structural capability of the panel to react a sustained load without failure to directly affect the ability of the concept UAV to perform a standard rate turn.

In order to reduce the magnitude of loading in anticipation for experimental testing, a section of the wing is chosen outboard at a location where the wing skin is sized for strength (further outboard the wing skin is sized by minimum gage or handling loads rather than flight loading). At a location roughly 260 inches outboard along the wing, the wing skin consisting of 4 plies of MTM45-1/AS4 carbon composite in a quasi-isotropic layup is necessary to meet the loading requirements due to FAR 23 design requirements, while not exceeding strain design allowable values for the plies. For the finite element models, a "cut-out" section of the wing is modeled. The relative location of this "cut-out" along the span of the wing is shown in Figure 13.

Three structural conditions were initially considered for the example panel: pristine, moderate, and severe damage. Damage cases are defined as delamination of the first ply, which is typical of a low-velocity impact on the panel or interlaminar separation caused by stress concentrations under

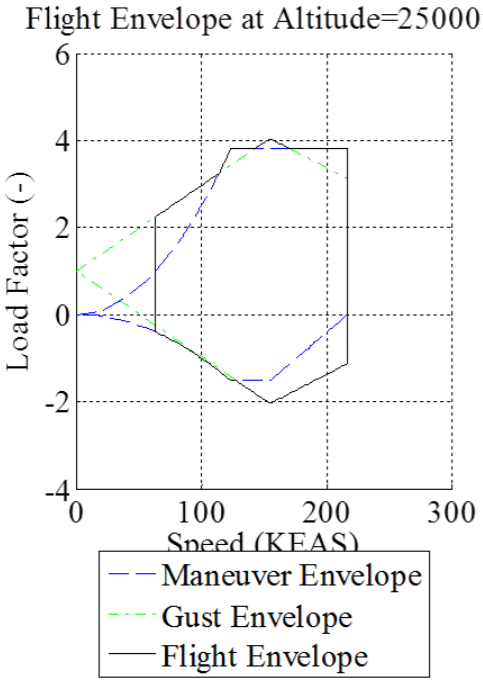

Figure 12: Flight envelope at an altitude of 25000 feet.

cyclic loading due to embedded foreign object debris or other defects. The panel conditions are modeled using the finite element method and strain values for the panel are estimated for a variety of loading conditions that can be traced back to loading from a variable turn rate. The level of delamination and resulting strain fields for the three conditions are shown in Figure 14. The images of the panel finite element model show the extent and location of the varying delamination size, where the red and light orange color indicates delamination between the first and second plies. The panels were reinforced around the boarders of the panel with through holes to simulate mounting the wing skins to the structure. The panel predicted strains indicate strain gradients that are expected to be present within the panel for the given loading. These sets of strains can then be used by the vehicle system to identify the condition of the panel based on measured strain values from strain gauges or other sensors on-board the vehicle. Once the panel condition is determined, the capability of the vehicle to perform a sustained turn necessary to follow a flight path can be determined and a go/no-go decision can be made.

The material properties used within the finite element models are provided by the material

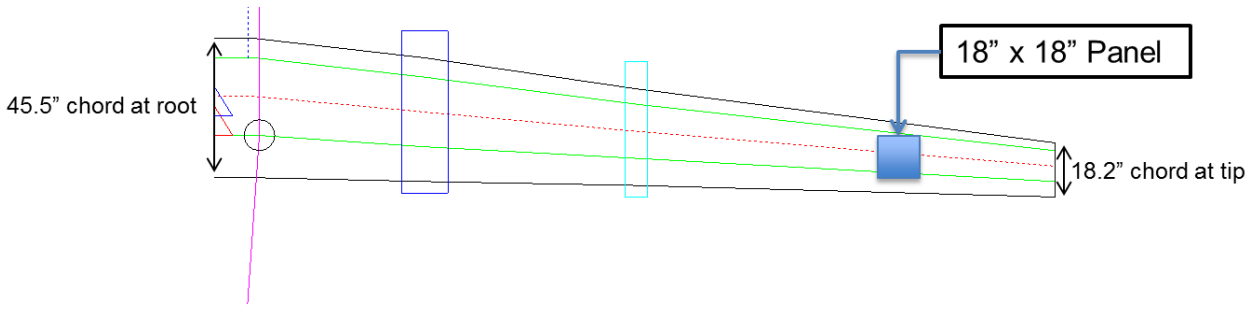

Figure 13: Relative location of the “cut-out” panel along the span of the wing.

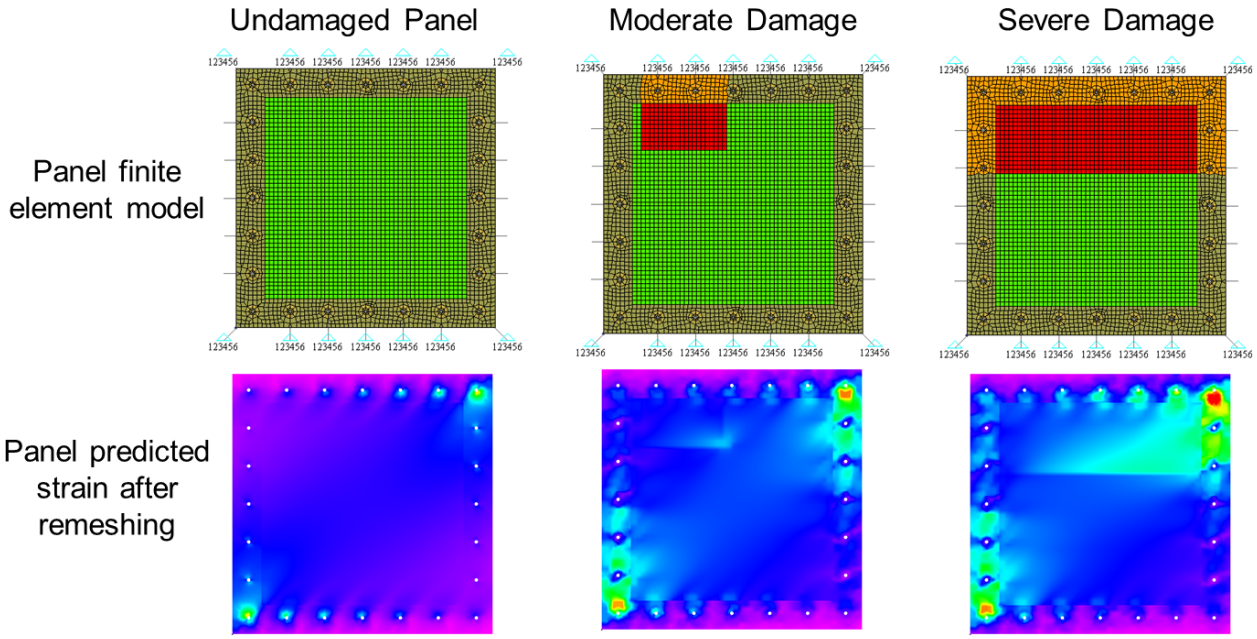

Figure 14: Finite element models and resulting strain fields for the three structural conditions.

manufacturer (www.umeco.com). To account for uncertainty within the finite element models, a normal distribution and coefficient of variance (Cv) of 5% is assumed and values corresponding to 99.86% confidence (3σ) are used. A summary of the properties is provided here:

- Composite properties:
  - Advantages: high strength/weight ratio; directional strength / stiffness tailoring; fatigue resistant
  - Disadvantages: more complex; brittle; most design allowables / testing is proprietary
  - MTM45-1/CF0525-36%RW, 193gsm 3K AS4 plain weave carbon fiber
    - Matrix: MTM45-1 flexible curing temperature, high performance, toughened epoxy matrix system optimized for low pressure, vacuum bag processing
    - Fiber: AS4 carbon fiber filaments made from PAN (polyacrylonitrile) precursor, surface treated; 3,000 filaments/tow
    - 36% Resin Weight (54.34% Fiber Volume)
    - 193 grams per square meter (gsm) areal weight (0.201 mm ply thickness)
    - Plain Weave warp and weft criss-cross in over-under pattern

2.4 Structural Response Model

A structural response model was created for the conceptual UAV using ASWING. ASWING is a program for the aerodynamic, structural, and control-response analysis of aircraft with flexible wings and fuselages of high to moderate aspect ratio. The program couples the structural and aerodynamical response of the vehicle. Thus, the loading on the aircraft wing can be investigated for different flight conditions. MATLAB scripts link the finite element models discussed in Section 2.3 with the ASWING models. The degradation of mechanical properties results in aerodynamic changes (i.e., shape of loaded wing will be different due to changes in structural response). The

coupled models allow for vehicle response to be investigated. The results from these coupled models indicate that the capability of the UAV will change between 2 and 12% (corresponding to strain levels within the panel changing between 1 and 20%) for the levels of structural damage investigated.

The model includes multiple degradation or failure modes including: damaged panel strength (BVID, thru-hole), damaged panel stiffness (BVID, thru-hole), loose fastener, fretted fastener hole, and disbonded surface. The algorithm is implemented in object-oriented MATLAB coding using handle classes for speed and compatibility with the following algorithmic elements:

- Framework (main.m)
  - Maintains "truth" data regarding flight, environment, and events (inputs)
- Inputs (Environment.m, MeasuredDamage.m, VehicleManeuver.m)
  - Measures inputs using sensors or flight controller; should include signal uncertainty, noise, and fault/failure models
  - Can be replaced by hardware-in-the-loop
- Algorithm (VehicleCapability.m)
  - Interrogates input classes and operates on the information to provide:
    - diagnostic information (Monitor method);
    - current or future vehicle state information (State method);
    - airframe capability (Capability method); and
    - prognostic information (Eval method)

Structural Modeling Routine

Tasks 2-4 are iterative.

1. Initialize
   - Read finite element model (nas file)
   - Generate nominal node map and element strength capability
2. Monitor(damage,environment)
   - Receive measured damage information (type, size, location)
   - Receive temperature information (gross temperature)
   - Modify local strength capability
   - Modify local stiffness or remesh (not implemented yet)
3. State(maneuver)
   - Export and run updated finite element model
   - Import finite element model stresses
   - Set current maneuver state
4. Capability

- Calculate finite element model failure indices against load cases
- Notch load cases based on reduced capability (not implemented yet)

5. Evaluate
    - Estimate Remaining Useful Life (RUL) using simulated load spectrum (not implemented yet)
    - Cost function information to decision making algorithms (not implemented yet)

Multiple diagnostic models can be integrated into the Monitor method. Error checking models can be integrated into the State method to compare updated model state predictions and additional sensors. Multiple prognostic models can be integrated into the Eval method, e.g., Sendeckyj/Whitworth residual strength models for composite fatigue and composite damage progression models for overloading conditions. A load spectrum generated using multiple loading scenarios generated by decision making agent to determine cost of short- and long-term operation. Current state and RUL estimates are then combined with updated usage scenarios.

2.5 Experimental Testing

Experimental testing was planned to follow model development. This was an additional activity that was not part of the original proposal; however, it was added because if the potential value in validating our modeling and algorithm contributions. As of the writing of this report, multiple experimental specimens containing different types of damage have been manufactured and a custom made load frame is under development. Testing of the specimens will occur as follow-on work at a later time.

The mechanical aspects of the load frame are complete, with all components assembled. Additional software development is required in order to control the load frame. The original goal was to have a table-top experiment. In order for the frame to supply loads large enough to damage the composite panels, the frame evolved to be a free-standing, self-reacting, load frame, as shown in Figure 15. The frame is still of a size that it can be transported and assembled on-site (unlike typical mechanical testers that require permanent installation). Quasi-dynamic tensile loading allows the loading experienced by the panel at the specified location on the wing and for specific vehicle maneuvers to be simulated. The load frame can apply uniaxial tensile loading. The "cut-out" section of the wing was selected such that uniaxial tension is a good approximation of the actual loading experienced. The magnitude of loading is to be directly related to executed maneuver. The software drivers will match the applied loading to anticipated loading resulting from maneuvers of the aircraft.

The load frame use a Duff-Norton worm gear actuator to impart load into the system. The actuator is rated for 5 tons (10000 lbf) and is driven via a DC motor. The motor is a Leeson 21 amp, 12 V-DC drive. An Elmo motion controller (DC-WHISTLE 20/60) controls the DC motor and interfaces with a personal computer in order to send control signals. A LabVIEW VI is under development to provide the motor control signals as well as record the data from the load cell and displacement sensor. The control will permit either load control or displacement control based on real-time data from the load cell or the LVDT, respectively. Controller feedback is provided via encoder (attached to actuator worm gear), LVDT, and/or load cell. The position sensor is a MacroSensors DC750-500 LVDT. The load cell is a Sensor Development 10188-014, 10 kip threaded rod load cell (uniaxial tensile load). The encoder is an Accu-Coder. The flight profile determined from the vehicle path planner will set the load path (load history). The load path will be executed in real-time, with real-time sensor data provided to the multi-fidelity models.

Figure 15: Load frame with composite specimen and DAQ system.

A National Instruments cDAQ system with multiple modules provides input/output control between the computer and the test instrumentation. One aspect that will be investigated before experimental testing is started is integrating optical strain measurements in order to measure full field strains, as opposed to single point measurements via strain gages.

The test specimens were manufactured at Aurora's Mississippi plant. Layups of four large panels were fabricated and sectioned into a total of 200 test specimens. While manufacturing these panels, two types of damage were included. Controlled areas of delamination were created by including teflon shapes between the first and second plies, as shown in Figure 16. The second form of damage was simulated fiber fracture that was implemented by cutting lengths of fibers within a single ply. The specimens were autoclave cured. An image of the panels placed within the autoclave after the cure cycle is shown in Figure 17.

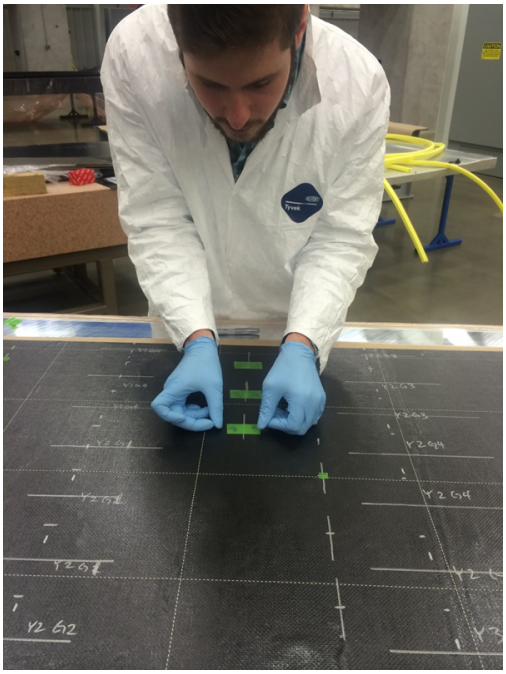

Figure 16: MIT graduate student Marc Lecerf places teflon inserts between plies to create delamination.

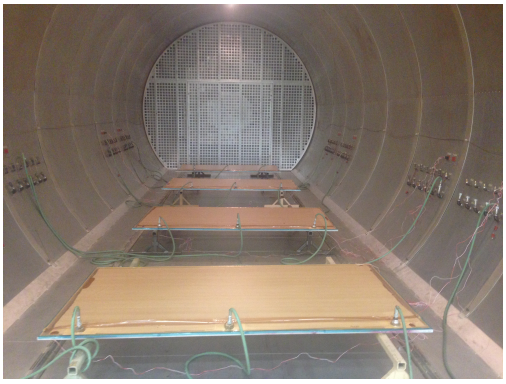

Figure 17: Panels being cured in Aurora's autoclave.

2.6 Multifidelity DDDAS Methods

Figure 18 shows our approach that combines offline computation with online sensor data to provide a time-constrained, updated estimate of UAV flight capability. More specifically, we combine information from physics-based models, simulated offline to build a scenario library, together with dynamic sensor data in order to estimate current flight capability. We also use dynamic data to modify our information-gathering strategies to manage uncertainty in our capability estimates.

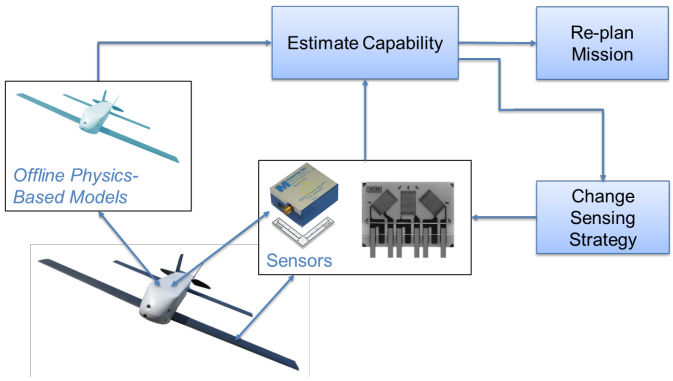

Figure 18: To achieve a self-aware vehicle capability, we use offline physics-based modeling combined with dynamic sensor data to achieve dynamically updated estimates of vehicle capabilities (e.g., the vehicle flight envelope).

2.6.1 Problem setup

We consider two kinds of quantities of interest:

- The quantities that are measured during flight, referred to as the *measured quantities of interest*. We denote these by $\mathbf{q}_m(\mathbf{x}),\ m = 1, \ldots, M$, where $\mathbf{q}_m$ is the mth measured quantity of interest (generally a vector representing a discretized field quantity) and we consider M such quantities.
- The quantities employed in the decision process that give information about capability and performance constraints, referred to as the *capability quantities of interest*. We denote these by $\mathbf{s}_c(\mathbf{x}),\ c = 1, \ldots, C$, where $\mathbf{s}_c$ is the cth capability quantity of interest (generally a vector representing a discretized field quantity) and we consider C such quantities.

Both quantities of interest are functions of the vehicle state, $\mathbf{x}$, which includes quantities describing the current damage state (e.g., damage location, extent and depth). In an offline phase, we use high-fidelity models to obtain detailed information about the system and its possible responses for different flight conditions and different damage states. The simulated information is stored in a damage library and is used to build a mapping from measured quantities of interest to capability quantities of interest via surrogate models. In the online phase, these surrogate models provide rapid estimates of vehicle capability given real-time measurements. The next two subsections describe in more detail the models and methods employed in our offline and online phases.

2.6.2 Offline stage

Our offline phase considers a suite of multifidelity physics-based models, at varying levels of physics resolution, and ranging from the panel level to the full vehicle level. We store offline analysis

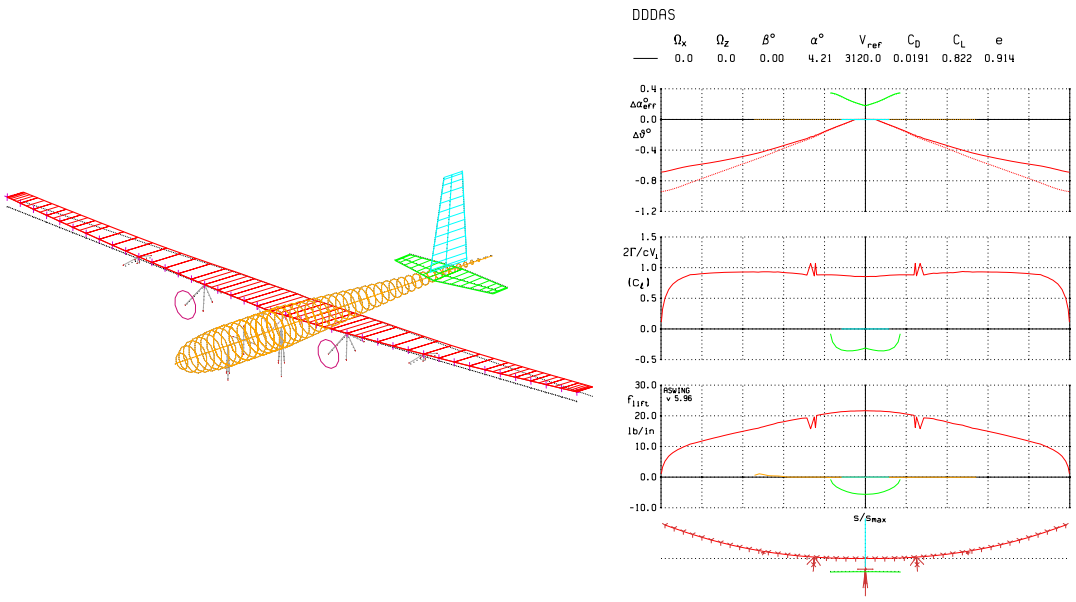

Figure 19: The representation of our concept UAV within ASWING. The structure is specified as a set of interconnected slender beams, where lifting surfaces have additional aerodynamic properties specified along their span. The plots to the right show the aeroelastic trim solution computed by ASWING for a pull-up maneuver at a fixed flight velocity and load factor.

information in a damage library. We use a variety of strategies to build surrogate models from this information, including support vector machines, proper orthogonal decomposition (POD) and self-organizing maps.

Vehicle-level models. At the vehicle level, a combination of ASWING [3] and the Variational Asymptotic Beam Cross-Sectional Analysis (VABS) [2] provides estimates of internal wing stresses and deflections as a function of input aircraft kinematic states and estimates of damage to the nominal aircraft structure.

ASWING [3] is a nonlinear aero-structural solver for flexible-body aircraft configurations of high to moderate aspect ratio. ASWING uses unsteady lifting line aerodynamics together with a finite difference Euler-Bernoulli beam structural model. The aerodynamic model is extended with Prandtl-Glauert compressibility treatment and a sectional stall model. The nonlinear Euler-Bernoulli beam model permits analysis of large deflections. Figure 19 shows the ASWING representation of our concept UAV and the corresponding aerostructural assessment for an example pull-up maneuver. The ASWING model is a set of interconnected slender beams—one each for the wing, fuselage, horizontal stabilizer, and vertical stabilizer. Lifting surfaces (the wing and stabilizers) have additional cross-sectional lifting properties that are pre-specified.

VABS [2] models the wing box as an array of two-dimensional cross-sectional finite element models. The cross-sections capture the details of a multi-ply composite wing skin and local damage effects. VABS computes lumped stiffness and inertial properties at a reference point in each cross section, forming a global line representation of the beam. A standard beam problem solver finds the global force and moment distribution along this reference line given input forces and moments. Using the reference line solution, the internal strain field can be recovered in the beam cross sections using relations initially computed by VABS. Figure 20 provides an overview of the VABS modeling framework. In this work, we use the specific UM/VABS implementation developed in FORTRAN

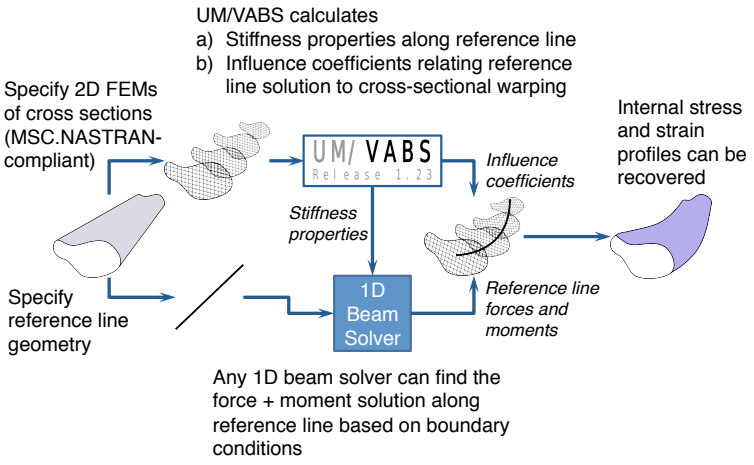

Figure 20: Variational Asymptotic Beam Cross-Sectional Analysis (VABS) allows for dimensional reduction of an expensive three-dimensional beam solution into two-dimensional finite element models coupled with an external beam solver.

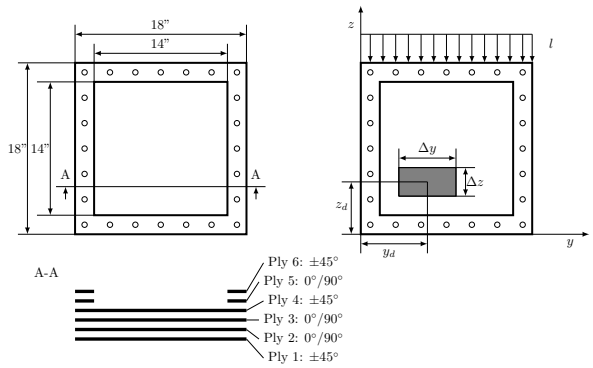

Figure 21: Panel layout and layer sequence. Panel state variables include the damage location, damage size, and load definition.

by R. Palacios and C. Cesnik at the University of Michigan [10].

In our integrated modeling setup, ASWING manages the one-dimensional beam solution, computing loads in the wing box for specific flight conditions, while VABS resolves local stiffness loss due to damage on the aircraft wing.

Panel-level models. At the panel level, we use a finite element model that simulates and analyzes the panel behavior under specified loading and damage scenarios using a plate model. The composite panel comprises carbon fiber plies with a specified stacking sequence. Four clamped edges define boundary conditions that simulate the presence of fastening bolts along the panel perimeter. Figure 21 shows a panel layout and corresponding panel cross-section for a case with four plies with the symmetric stacking sequence $[\pm 45°, 0°/90°, 0°/90°, \pm 45°]$. The border area that hosts the holes is reinforced with two additional plies with orientation $0°/90°$ and $\pm 45°$. The grey shaded area on the right plot of Figure 21 denotes the damaged region, which is centered at (y_d, z_d) and has extent $\Delta y \times \Delta z$.

The loads l on the panel are defined by the prescribed aircraft maneuver. The presence of damage is simulated by weakening the stiffness properties of the finite elements that belong to the prescribed damaged area. This model is used to explore different damage scenarios. For each scenario, we generate a snapshot set by evaluating the measured quantities of interest and the capability quantities of interest. The measurement quantities of interest are the components of strain evaluated for each element in the computational mesh. The capability quantities of interest are the failure indices, also evaluated for each element in the computational mesh. Failure index is an indicator of the structural condition that is translated into a scaling factor for maneuver parameters. It is defined as the ratio between the experienced stress and the maximum allowable stress (typically the compression/tension/shear strength that characterizes the material properties).

Damage library. The purpose of the damage library is to store information from analyses run offline using the panel-level and vehicle-level models. This information may be accessed by online analyses in a variety of different ways (e.g., directly accessing the predictions associated with a damage scenario, or using library entries to perform dynamic adaptation of a reduced-order model). The damage library is populated by offline analysis of a range of damage scenarios and kinematic states relevant to the planned mission of the vehicle. Information regarding the planned mission can be used to determine the type of damage that may occur and the types of maneuvers that may be performed. This information, along with resource constraints on the library, can be used to optimize the contents of the damage library given mission level objectives. In our current implementation, the library contains model predictions of sensed strain and maximum failure indices for each scenario considered. Ongoing work is investigating the utility of including model predictions of other quantities.

Classification and surrogate modeling. We embody the information generated by these physics-based models using various surrogate modeling techniques. At the panel level, we build low dimensional representations of the measured and capability quantities of interest, using the POD. We then use self-organizing maps to cluster the resulting data and to build a surrogate model that maps measurements to capability estimates. The steps in this process are outlined in Figure 22. The details of the panel-level approach are described in [8].

At the vehicle level, we use the maximum computed failure index to classify all simulated conditions into safe (maximum failure index < 1) and unsafe (maximum failure index ≥ 1). We build a representation of the failure boundary (maximum failure index $= 1$) as a function of damage parameters and vehicle operating conditions. Our current implementation uses a simple bisection method to define the failure boundary; future work will use adaptive sampling with support vector machines as in [4]. The steps in this process are outlined in Figure 23 and are described in more detail in [7].

2.6.3 Online stage

In the online stage, our goal is to move from sensed data to updated estimates of structure capability at the local panel level and updated flight envelopes at the vehicle level. The key is to achieve these estimates sufficiently rapidly to support dynamic decision-making, while leveraging the rich amount of physics-based information contained within our damage library. We also aim to characterize our level of confidence in our updated estimates.

At the panel level, the low-dimensional POD representations combined with the self-organizing map clustering achieve the desired rapid assessment. Figure 22 shows the online flow of analysis

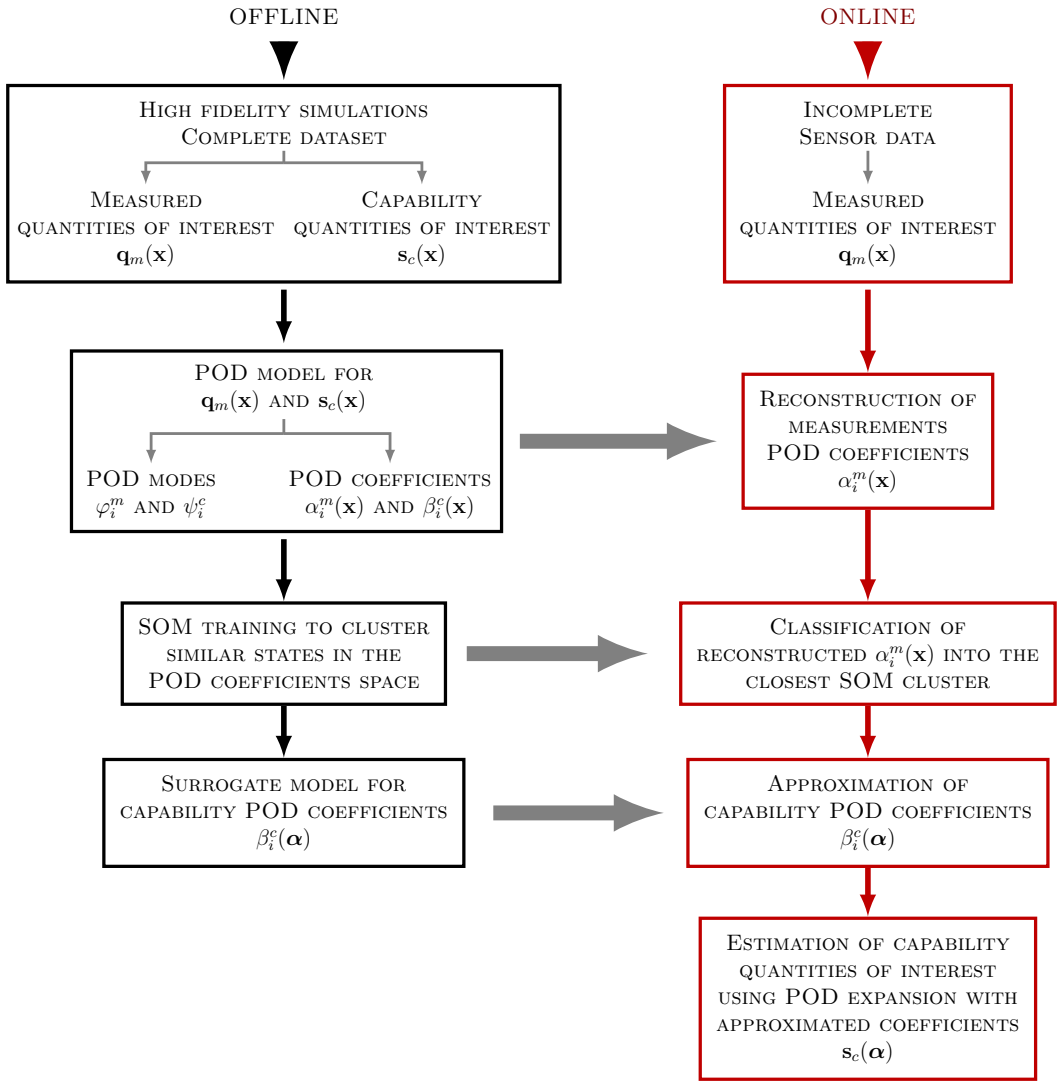

Figure 22: Diagram of the offline (black boxes) and online (red boxes) steps of our approach at the panel level. POD models and clusters are obtained offline and employed online as indicated by the gray arrows.

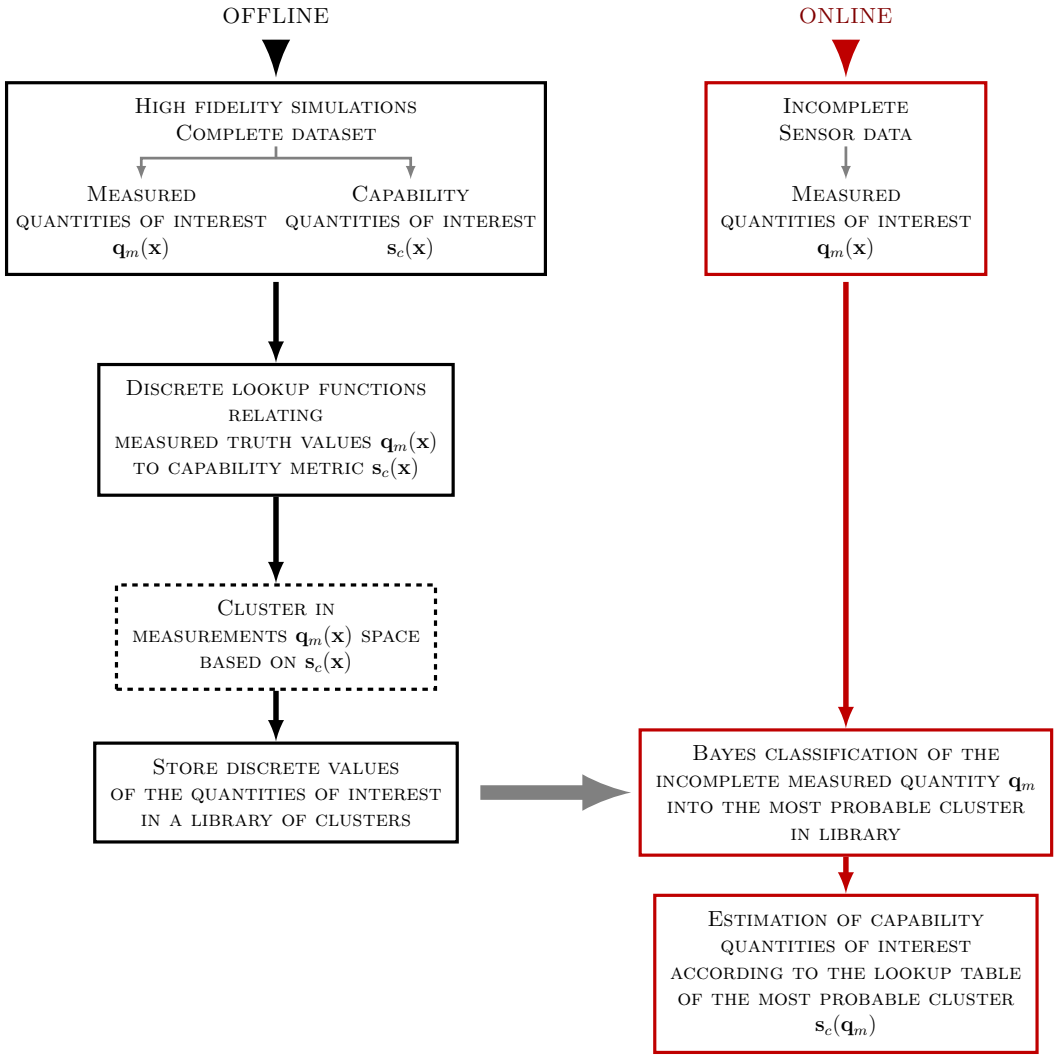

Figure 23: Diagram of the offline (black boxes) and online (red boxes) steps of our approach at the vehicle level. Damage library information is stored using offline clustering based on the capability quantities of interest. The library information is employed online using a Bayes classifier as indicated by the gray arrow.

that moves from sensed strain data to estimates of panel failure indices. The reconstruction of the POD coefficients in the second step is achieved using the gappy POD approach [1, 5].

At the vehicle level, we use a Bayes classifier that assigns a posterior estimate of the probability of being in any damage state contained in our damage library. A simple approach, described in [7], assigns equal prior probability to each damage state in the library and classifies the vehicle's damage state as the state in the library with the maximum posterior probability. A more sophisticated approach incorporates mission information, current maneuver, and a mixture model of the posterior damage state. The additional mission and maneuver information permit us to relax the assumption of equal prior damage state probabilities. The mixture model of the posterior damage state enables interpolation among records in the damage library, permitting us to characterize a richer range of vehicle damage states.

2.6.4 Results

The offline vehicle model allows for determination of the vehicle capability over a range of damage events using classification. Figure 24 shows an example of this process. We simulate a pull-up maneuver at constant velocity $V = 260$ ft/s with varying load factor $n \in [1, 3.5]$ over a range of two chordwise damage size parameters, with fixed spanwise size parameters and constant depth. Each damage and maneuver combination is classified as "safe" or "unsafe" based on the value of the maximum failure index in the wing structure. Using this classifier variable, the boundary surface between safe and unsafe maneuver regions for any given damage case can be determined using a bisection algorithm.

Figure 25 presents results for an example case at the panel level. The surrogate models are obtained offline using an evaluation set of 3000 different damage cases for fixed panel layout and loading condition (Figure 21). We show here results for the case of a 3.5220×7.7540 square-inch damage located at ($y_d = 10.5900$, $z_d = 12.9100$) and involving plies 4, 5 and 6. The figure shows the original finite element solution for the failure index field over the panel. We use this solution to generate synthetic data with which to test our approach. The bottom right plot of Figure 25 shows the corresponding online estimate of the failure index given by our surrogate modeling approach, reconstructed using strain sensor measurements that cover 50% of ply 4. The other two plots in Figure 25 are included to give insight to the errors due to the POD approximation and the self-organizing map as follows. The top right plot represents the best approximation of the original finite element solution in the POD basis—this would be achieved only if we could reconstruct the POD modal coefficients exactly. The bottom left plot shows that a small amount of additional error is introduced by using the self-organizing map to map from POD measurement coefficients to POD capability coefficients. The final plot in the lower right also includes the error due to inferring the POD measurement coefficients from sparse data. Overall, the reconstructions of the failure indices are sufficient to provide a first-cut assessment for online decision-making.

We also present representative results at the vehicle level. One potential application of our method is for missions in contested environments, where threats to the vehicle due to hostile agents require a fast, defensive reaction to avoid dangerous regions of the flight zone. In addition, the vehicle may sustain damage on the wing surface that impedes its ability to operate at its initial design capability. Figure 26 presents a schematic of this scenario, where the vehicle initiates the evasive action at an airspeed of 210 ft/s and an initial load factor of 1.3 (representative of a nominal maneuvering speed and an upper bound on the nominal maneuvering load factor during normal operation while navigating a sequence of waypoints).

We demonstrate how the decision strategy, informed by the capability estimate, trades off between survivability and full utilization of the vehicle capability. For details on these results,

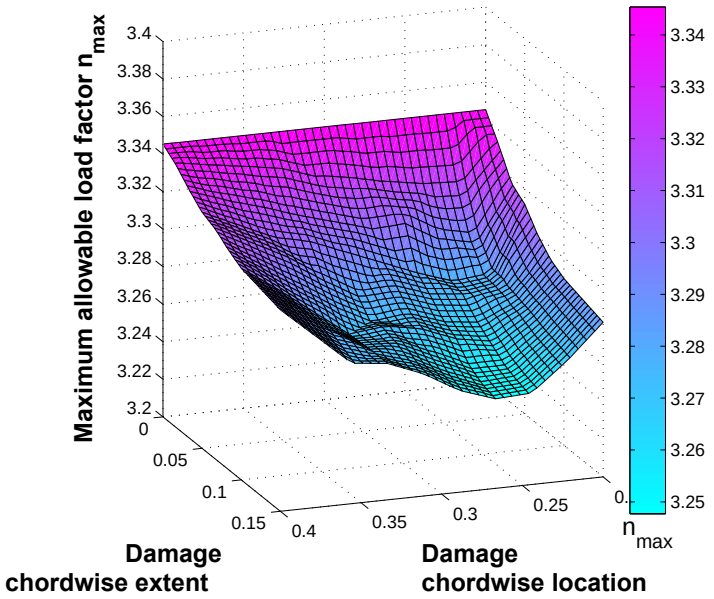

Figure 24: Surface representing the vehicle capability as a function of two damage parameters using the offline vehicle model. A pull-up maneuver with constant velocity V and varying load factor n produces wing loading cases that are classified as safe or unsafe, producing a maximum safe load factor n_{max} for each damage case using a bisection algorithm. Note that when the chordwise damage extent is zero, the damage region is degenerate with zero volume, and the model operates using the baseline "pristine" aircraft configuration; hence, we see no change to the maximum allowable load factor.

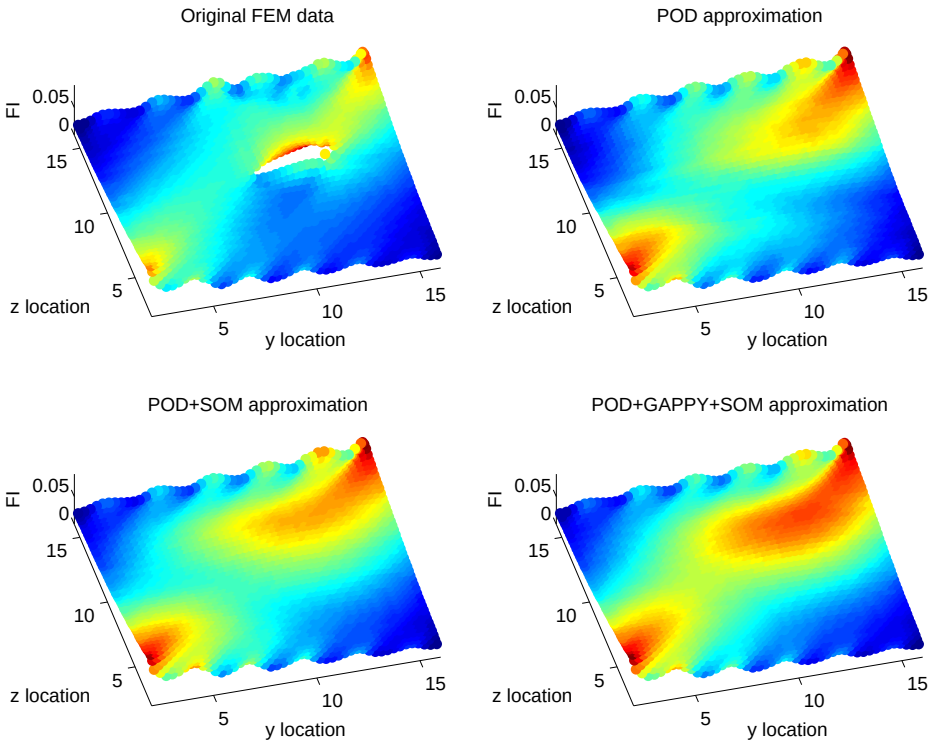

Figure 25: Failure index *FI* over the panel. The panel border containing the bolt holes is excluded for plotting clarity. Top left: the "truth" finite element model (FEM) solution. Top right: the representation of the FEM solution in the POD basis. Bottom left: POD approximation combined with self-organizing map (SOM) surrogate, mapping measurement POD coefficients to capability POD coefficients. Bottom right: our full approach using gappy POD to infer POD coefficients from measured data, and SOM to map from measurement POD coefficients to capability POD coefficients.

see [6, 7]. We quantify survivability by evaluating probability of maneuver success over all possible damage cases. We quantify utilization using the average ratio between the vehicle's operational load factor and the vehicle's true maximum load factor.

The probability of maneuver success, $\mathbf{p}(MS)$, is defined as the probability that the agent chooses a value of operating load, n_{op}, that is less than the maximum vehicle load factor n_{max}^{truth}. The utilization is defined as the average ratio between the vehicle's operational load factor and the vehicle's true maximum load factor. Figure 27 plots the probability of maneuver success, $\mathbf{p}(MS)$, versus the utilization, $\bar{n}_{util}$, for the two decision strategies: a static estimate based on the vehicle design flight envelope, and our DDDAS strategy that uses a dynamic estimate of the vehicle structural capability based on dynamic strain data. A third curve is plotted that shows the performance of a hypothetical estimator that knows the damage case with absolute certainty; that is, its only error is due to the surrogate model approximation of the corresponding capability set (in this case using a probabilistic support vector machine).

The ideal decision strategy would have both perfect usage of available capability (i.e., $\bar{n}_{util} = 1$) and certain maneuver success (i.e., $\mathbf{p}(MS) = 1$); this is marked as the "Utopia" point in the upper right corner of Figure 27. A sample on the plot is considered to be *non-dominated* if no other sample has both a higher $\mathbf{p}(MS)$ and higher $\bar{n}_{util}$ value (or higher value of one and equal value of the other); the non-dominated combinations of $(n_{util}, \mathbf{p}(MS))$ for each estimator are connected by

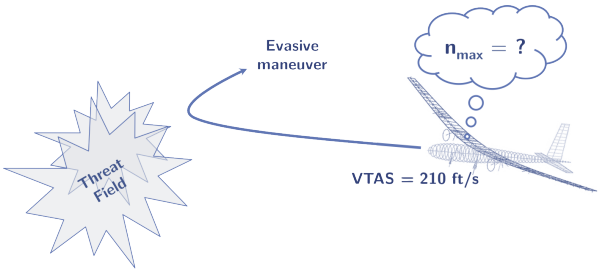

Figure 26: Schematic of the flight scenario to which we apply our DDDAS capability estimation framework.

a dashed line of the corresponding color.

Figure 27 shows that the static capability case has $\mathbf{p}(MS) = 1$ at values of $\bar{n}_{util} < 0.75$. This is because if the agent sets a sufficiently low static load factor, the realized load is less than n_{max}^{truth}. Thus, within the scope of our analysis the vehicle never exceeds the flight envelope, although the loads are limited to conservative values and utilization is low. The figure also shows that the static capability case has a long trail of samples near $\mathbf{p}(MS) = 0$ at high values of $\bar{n}_{util}$. This is because at values of n_{op}^{static} close to 2.9, the vehicle almost certainly exceeds the flight envelope unless it is in the pristine case, which has a small probability (< 0.01) of occurring. We see that the dynamic estimator results in an even spread of points across the non-dominated front, with a sharp "knee" at $\bar{n}_{util} \approx 0.95$ where the probability of maneuver success drops rapidly.

We can use the non-dominated fronts Figure 27 as a measure of performance of each capability estimate when used for decision-making in the flight scenario. For instance, if the agent wants to utilize 95% of the maximum vehicle load factor on average, there would be an 80% chance of maneuver success using the dynamic estimate of the load factor as opposed to a 40% chance of success when operating at a static load factor. On the other hand, if the agent can accept operating at less than 80% of the maximum capability on average, then both estimators show similar performance. We note this is most likely because the damage cases in the library cause a limited reduction in the vehicle capability, and simulating more severe damage cases would continue to emphasize the performance gain from using the dynamic capability estimate. Lastly, Figure 27 shows that if the damage were known perfectly, the error introduced by the surrogate modeling approximations would be relatively small for this example. The difference between the dynamic capability curve and the known damage curve is an indication of the value (in terms of vehicle capability utilization and maneuver success probability) of increased quality and quantity of sensors. Comparisons of this kind could be used to support design decisions regarding the cost versus value tradeoffs of including more onboard sensors.

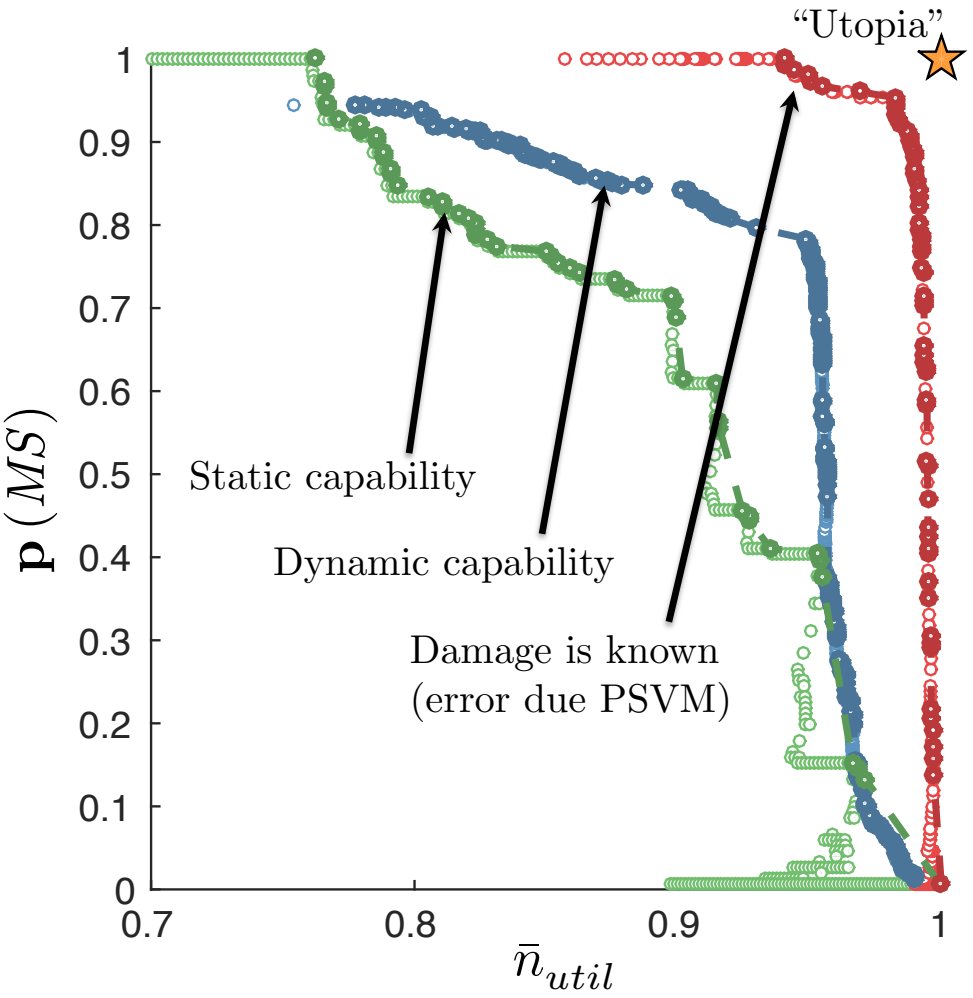

Figure 27: The probability of maneuver success ($\mathbf{p}\,(MS)$) versus the average fraction of the vehicle capability utilized ($\bar{n}_{util}$) for an onboard decision process performed by an agent using either a static or dynamic capability estimation strategy. Also plotted is a hypothetical capability estimate that knows the damage with certainty but still uses a PSVM capability approximation. The non-dominated points for each capability estimation strategy are connected by a dashed line of the corresponding color.

2.7 Fast parallel algorithms for data assimilation using Bayesian approaches

Aircraft state characterization technologies require fast algorithms for the solution of inverse medium problems for damage characterization. Assuming a known constitutive law for the mechanical response of a "healthy" structure, one can solve an inverse medium problem to find perturbations in the material properties that appear in the the constitutive law.

Such problems can be formulated as inverse medium problems. We consider their general formulation in a Bayesian setting. In particular we considered an idealized inverse medium problem that models the reconstruction of the unknown structure state of an aircraft given partial observations of the state. For that we considered fast algorithms for deterministic inverse problems, construction of likelihood and prior probability functions for spatial field, and kernel density estimation.

Below we discuss some representative results from work partially funded by this award.

- We developed a new algorithm for fast kernel density estimation in high dimensions summarized in [9]. A direct evaluation of the sum scales quadratically with the number of points. Fast kernel summation methods can reduce this cost to linear complexity, but the constants involved do not scale well with the dimensionality of the dataset. The main algorithmic components of fast kernel summation algorithms are the separation of the kernel sum between near and far field (which is the basis for pruning) and the efficient and accurate approximation of the far field. We introduced novel methods for pruning and approximating the far field. Our far field approximation requires only kernel evaluations and does not use analytic expansions. Pruning is not done using bounding boxes but rather combinatorially using a sparsified nearest-neighbor graph of the input. The time complexity of our algorithm depends linearly on the ambient dimension. The error in the algorithm depends on the low-rank approximability of the far field, which in turn depends on the kernel function and on the intrinsic dimensionality of the distribution of the points. The error of the far field approximation does not depend on the ambient dimension. We presented the new algorithm along with experimental results that demonstrate its performance. We report results for Gaussian kernel sums for 100 million points in 64 dimensions, for one million points in 1000 dimensions, and for problems in which the Gaussian kernel has a variable bandwidth. To the best of our knowledge, all of these experiments are impossible or prohibitively expensive with existing fast kernel summation methods.

- We developed fast algorithms for Bayesian inverse medium problems [12]. We consider a supervised inverse medium problem algorithm using a Bayesian framework and a variational formulation for a maximum a posteriori (MAP) estimation of the label field. In the Bayesian framework, we must define the likelihood function (the probability of the data given the label field) and the prior probability (for the label field). In this work, we focus on the likelihood. Typically, the likelihood of the intensity is decoupled for every inverse medium point and is given by a parametric density (often a Gaussian function). Instead, we propose a non-parametric, high-dimensional, kernel density estimation (KDE) for the likelihood function, based on Gabor features (300 per pixel). This approach better approximates non-local correlations. For the prior function, we use a simple smoothness prior. We provide experimental evidence that this likelihood function performs very well and converges to the correct segmentation with the number of training datasets.

3 Publications

1. D. Allaire, G. Biros, J. Chambers, O. Ghattas, D. Kordonowy and K. Willcox, *Dynamic Data Driven Methods for Self-aware Aerospace Vehicles*, Procedia Computer Science, Vol. 9, pp. 1206–1210, 2012

2. D. Allaire, G. Biros, J. Chambers, O. Ghattas, D. Kordonowy and K. Willcox, *An Offline/Online DDDAS Capability for Self-Aware Aerospace Vehicles*, Procedia Computer Science, Vol. 18, pp. 1959–1968, 2013

3. D. Allaire, D. Kordonowy, M. Lecerf, L. Mainini and K. Willcox, *Multifidelity DDDAS Methods with Application to a Self-Aware Aerospace Vehicle*, Procedia Computer Science, Vol. 29, pp. 1182–1192, 2014

4. A. Gholami, D. Malhotra, H. Sundar, and G. Biros, *FFT, FMM, or multigrid? A comparative study of state-of-the-art Poisson solvers*, SIAM Journal on Scientific Computing, in review
`http://arxiv.org/abs/1408.6497`

5. A. Khawaja, J. Wang, D. Malhotra, A. Gerstlauer, G. Biros and L. John, *Performance Analysis of HPC Applications with Irregular Tree Data Structures*, Proceedings of the 20th IEEE International Conference on Parallel and Distributed Systems (ICPADS 2014), IEEE, Hsinchu, Taiwan, December 2014

6. D. Kordonowy, J. Chambers, and R. Cowlagi, *Contingency Management for Condition-Aware Unmanned Aerial Vehicles*, AIAA 2013-5215, presented at AIAA Infotech@Aerospace, Boston, MA, August 2013

7. M. Lecerf, D. Allaire, K. Willcox, and D. Kordonowy, *A Dynamic Data Driven Approach to Online Flight Envelope Updating for Self Aware Aerospace Vehicles*, AIAA-2014-1175, in Proceedings of 16th AIAA Non-Deterministic Approaches Conference, National Harbor, MD, January 13–17, 2014

8. M. Lecerf, D. Allaire and K. Willcox, *Methodology for Dynamic Data-Driven Online Flight Capability Estimation*, under review (second round), AIAA Journal

9. M. Lecerf, *A Data-Driven Approach to Online Flight Capability Estimation*, SM Thesis, Massachusetts Institute of Technology, June 2014

10. L. Mainini and K. Willcox, *A surrogate modeling approach to support real-time structural assessment and decision-making*, accepted for publication, AIAA Journal. Also AIAA-2014-1488, presented at 10th AIAA Multidisciplinary Design Optimization Conference, National Harbor, MD, January 2014

11. L. Mainini and K. Willcox, *Sensitivity analysis of surrogate-based methodology for real-time structural assessment*, AIAA paper, in Proceedings of AIAA Modeling and Simulation Technologies Conference, Kissimmee FL, January 2015

12. D. Malhotra and G. Biros, *PvFMM: A distributed memory fast multipole method for volume potentials*, ACM Transactions on Mathematical Software,
`padas.ices.utexas.edu/static/papers/pvfmm.pdf`

13. D. Malhotra, A. Gholami, and G. Biros, *A volume integral equation Stokes solver for problems with variable coefficients*, Proceedings of SC2014, IEEE/ACM, New Orleans, LA, November 2014, (**Best Student Paper Finalist**)

14. W. B. March and G. Biros, *Far-Field Compression for Fast Kernel Summation Methods in High Dimensions*, SIAM Journal on Scientific Computing, in review
`http://arxiv.org/abs/1409.2802`

15. W. B. March, B. Xiao, and G. Biros, *ASKIT: Approximate Skeletonization Kernel-Independent Treecode in High Dimensions*, SIAM Journal on Scientific Computing, in review
`http://arxiv.org/abs/1410.0260`

16. B. Peherstorfer and K. Willcox, *Dynamic Data-Driven Reduced-Order Models*, accepted for publication, Computer Methods in Applied Mechanics and Engineering, 2015.

17. B. Peherstorfer and K. Willcox, *Detecting and adapting to parameter changes for reduced models of dynamic data-driven application systems*, accepted for publication, Proceedings of International Conference on Computational Science (ICCS), 2015.

18. B. Peherstorfer and K. Willcox, *Online Adaptive Model Reduction for Nonlinear Systems*, submitted, SIAM Journal on Scientific Computing, 2014.

19. H. Sundar, G. Biros, C. Burstedde, J. Rudi, O. Ghattas and G. Stadler, *Parallel Geometric Multigrid Methods on Unstructured Forests of Octrees*, Proceedings of SC2012, IEEE/ACM, Salt Lake City, UT, November 2012

20. H. Sundar, D. Malhotra, and G. Biros, *HykSort: a new variant of hypercube quicksort on distributed memory architectures*, ACM International Conference on Supercomputing, Eugene, Oregon, June 2013

21. H. Sundar, G. Stadler and G. Biros, *Comparison of Multigrid Algorithms for High-order Continuous Finite Element Discretizations*, Linear Algebra and Its Applications, in review
`http://arxiv.org/abs/1402.5938`

22. B. Xiao and G. Biros, *A High-dimensional Kernel Density Estimation-based likelihood function for Bayesian image segmentation*, in review

4 Presentations

1. D. Allaire. Offline libraries and online classification for enabling a dynamic data-driven self-aware aerospace vehicle, ASME IDETC Dynamic Data-Driven Application Systems Panel Session, Buffalo, NY (August 2014).

2. D. Allaire. An offline/online approach to enabling a dynamic data-driven self-aware aerospace vehicle, MIT DDDAS Workshop, Cambridge, MA (May 2014).

3. G. Biros, Fast algorithms for the evaluation for volume integral equations on hybrid ar- chitectures, Keynote Workshop: Exploiting Different Levels of Parallelism for Exascale Computing, ACM International Conference on Supercomputing, Munich, Germany (June 2014).

4. G. Biros, N-body algorithms in computational science and engineering, Institute for Advanced Studies Colloquium, Technical University of Munich, Munich, Germany (June 2014).

5. G. Biros, Parallel hierarchical algorithms for volume integral equations, Scalable Hierarchical Algorithms for eXtreme Computing-2 Workshop, King Abdullah University of Science and Technology, Saudi Arabia (May 2014).

6. G. Biros, Scalable Nearest Neighbor Search Algorithms in High Dimensions, Data-centered and Grid-based Non-parametric Probability Density Estimation minisymposium, SIAM Conference on Uncertainty Quantification, Savannah, GA (March 2014).

7. G. Biros, Scalable algorithms for the evaluation of volume potentials, University of Michigan, Colloquium series, Department of Mathematics, Ann Arbor, MI (March 2014).

8. G. Biros, N-body algorithms in computational physics and statistical inference, Department of Informatics Colloquium, Technical University of Munich, Munich, Germany (June 2013).

9. G. Biros, Supervised learning algorithms for construction of likelihood and prior densities for Bayesian inverse medium problems, Workshop on large-scale inverse problems and quantification of uncertainty: big data meets big models, Santa Fe, NM, (May 2013).

10. G. Biros, H-FaIMS: A hierarchical fast inverse medium solver, SIAM Conference on Computational Science and Engineering, Boston, MA (February 2013).

11. D. Kordonowy, Toward a more Autonous Unmanned Vehicle: How technology can give drones feeling and what they can do with it, Worcester Polytechnic Institute Mechanical Engineering Seminar Series, Worcester, MA (September 2013).

12. L. Mainini, K. Willcox. Real-time data-to-decision using adaptive surrogate modeling strategies. 2015 SIAM Conference on Computational Science and Engineering. Salt Lake City, UT (March 2015).

13. L. Mainini, K. Willcox. Sensitivity analysis of surrogate-based methodology for real-time structural assessment. 56th AIAA/ASCE/AHS/ASC Structures, Structural Dynamics, and Materials Conference, AIAA SciTech 2015. Kissimmee, Florida (January 2015).

14. L. Mainini, K. Willcox. A non-intrusive adaptive strategy to support real-time structural assessment. RAeS 4th Aircraft Structural Design Conference 2014. Belfast, UK (October 2014).

15. L. Mainini, K. Willcox. Data-driven reduced-order modeling to support online decision-making for self-aware aircraft. 11th World Congress on Computational Mechanics. Barcelona, Spain (July 2014).

16. L. Mainini, K. Willcox. A surrogate modeling approach to support real-time structural assessment and decision-making. 10th AIAA Multidisciplinary Design Optimization Conference, AIAA SciTech 2014. National Harbor, Maryland (January 2014).

17. D. Malhotra, A Volume Integral Equation Solver for Boundary Value Problems with Highly Heterogeneous Coefficients, 16th SIAM Conference on Parallel Processing for Scientific Computing, Portland, OR (February 2014).

18. D. Malhotra and G. Biros, A Distributed-Memory Fast Multipole Method for Volume Potentials, finalist, ACM Student Research Competition, ACM/IEEE SC13, Denver CO (November 2013).

19. B. March, Efficient, Scalable Algorithms for N-Point Correlation Functions, 16th SIAM Conference on Parallel Processing for Scientific Computing, Portland, OR (February 2014).

20. B. Peherstorfer. Online Adaptive Model Reduction. SIAM Conference on Computational Science and Engineering 2015. Salt Lake City, UT (March 2015).

21. B. Peherstorfer. Nonlinear model reduction through online adaptivity and dynamic models. Scientific Computing Colloquium. Technical University Munich, Munich, Germany (December 2014).

22. B. Peherstorfer. Sparse grid density estimation with data independent quantities. Sparse Grids and Applications 2014. University of Stuttgart, Stuttgart, Germany (September 2014).

23. B. Peherstorfer. Density Estimation with Adaptive Sparse Grids for Large Datasets. SIAM Data Mining 2014. Philadelphia, PA (April 2014).

24. B. Peherstorfer. Density Estimation with Adaptive Sparse Grids. SIAM Uncertainty Quantification 2014. Savannah, GA (April 2014).

25. H. Sundar, Nested Partitioning Scheme for Adaptive Meshes on Parallel Heterogeneous Clusters, 16th SIAM Conference on Parallel Processing for Scientific Computing, Portland, OR (February 2014).

26. K. Willcox. Reducing, Learning, and Adapting Models: Data-driven Model Reduction Approaches. Santa Fe Institute, Santa Fe, NM (March 2015).

27. K. Willcox. Data-driven model reduction to support decision making in complex systems. Invited minisymposium, SIAM Conference on Computational Science and Engineering, Salt Lake City, UT (March 2015).

28. K. Willcox. Multifidelity modeling: Exploiting structure in high-dimensional problems. Workshop on Numerical Methods for High-dimensional Problems. Ecole des Ponts Paristech, Paris, France (April 2014).

29. K. Willcox. Model Reduction for Large-Scale Systems. Tufts SIAM Student Chapter, Tufts University, Cambridge, MA (February 2014).

30. K. Willcox, Multifidelity Modeling for Design, Optimization and Uncertainty Quantification, Department of Mechanical Engineering Colloquium, McGill University, Montreal (October 2013).

31. K. Willcox, Multifidelity Modeling for Design, Optimization and Uncertainty Quantification, Department of Informatics Kolloquium, TU Munich (September 2013).

32. K. Willcox, Multifidelity Modeling for Aircraft Design and Optimization, Boeing Distinguished Researcher and Scholar Seminar, Huntington Beach, CA, August 2013. (invited)

33. B. Xiao, Parallel Algorithms For Nearest Neighbor Searches, 16th SIAM Conference on Parallel Processing for Scientific Computing, Portland, OR (February 2014).

5 Transitions

- Willcox hosted a DDDAS Collaboration Meeting at MIT in May 2014. The meeting brought together a small group of DDDAS researchers with local industry and government participants, with a focus on applications in the aerospace domain. The goals of the meeting were: (1) to identify potential beneficial opportunities to transition existing DDDAS methods and algorithms, including potential future collaborations, and (2) to discuss open challenges in managing the data-to-decisions flow in future aerospace systems. Government and industry participants included AFRL, Lincoln Laboratories, Draper Laboratories, Raytheon, and Aurora Flight Sciences. The meeting resulted in productive discussions and identified several avenues for future collaborations among academic and industry/government participants.

- The aircraft design framework developed in part under this research has been used by designers at Aurora Flight Sciences to conduct a large number of design studies, in which rapid turnaround of a feasible configuration and performance estimates were required. Aurora have further built upon these toolsets to include several levels of fidelity and to allow implementation of a large number of multidisciplinary design optimization (MDO) algorithms.

- Aurora Flight Sciences have an ongoing Air Force SBIR effort that has just reached the end of Phase I (we are working on Phase II proposal) that continues to develop/realize the self-aware vehicle concept. The effort has focused on the framework that connects/informs an in-situ mission planner of the capability of multiple subsystems of a vehicle. Because of the DDDAS effort, our technical effort in this SBIR has focused on developing the engine health/degradation models and the interface control with the mission planner. The research has been directed such that we can plug in the DDDAS structural results down the line. The DDDAS effort is a key component necessary for our framework to work.

6 Supported personnel

Aurora Flight Sciences: Jeffrey Chambers, David Kordonowy.

Massachusetts Institute of Technology: Graduate Students: Marc Lecerf (now at Raytheon). Postdoctoral Researchers: Laura Mainini, Benjamin Peherstorfer, Demet Ulker. Research Scientist: Douglas Allaire (now at Texas A&M University). Undergraduate Researcher: Harriet Li.

University of Texas: Graduate Students: Dhairya Malhotra, Bo Xiao, Amir Gholami. Postdoctoral Researchers: Hari Sundar (now at University of Utah), Bill March.

References

[1] T. Bui-Thanh, M. Damodaran, and K. Willcox, *Aerodynamic data reconstruction and inverse design using proper orthogonal decomposition*, AIAA Journal, 42 (2004), pp. 1505–1516.

[2] C. E. S. Cesnik and D. H. Hodges, *Vabs: A new concept for composite rotor blade cross-sectional modeling*, Journal of the American Helicopter Society, 42 (1997), pp. 27–38.

[3] M. Drela, *Integrated simulation model for preliminary aerodynamic , structural , and control-law design of aircraft*, in Proceedings of the 40th AIAA SDM Conference, no. AIAA Paper 99-1394, St. Louis, MO, Apr. 1999, American Institute of Aeronautics and Astronautics.

[4] C. Dribusch and S. Missoum, *Construction of aeroelastic stability boundaries using a multi-fidelity approach*, in 53rd AIAA/ASME/ASCE/AHS/ASC Structures, Structural Dynamics and Materials Conference 20th AIAA/ASME/AHS Adaptive Structures Conference 14th AIAA, no. AIAA Paper 2012-1803 in Structures, Structural Dynamics, and Materials and Co-located Conferences, Reston, Virginia, Apr. 2012, American Institute of Aeronautics and Astronautics.

[5] R. Everson and L. Sirovich, *The Karhunen-Loève procedure for gappy data*, Journal of Optical Society of America, 12 (1995), pp. 1657–1664.

[6] M. Lecerf, *A data-driven approach to online flight capability estimation*, master's thesis, MIT, June 2014.

[7] M. Lecerf, D. Allaire, K. Willcox, and D. Kordonowy, *A dynamic data driven approach to online flight envelope updating for self aware aerospace vehicles.* AIAA-2014-1175, in Proceedings of 16th AIAA Non-Deterministic Approaches Conference, National Harbor, MD, January 13–17, 2014.

[8] L. Mainini and K. Willcox, *A surrogate modeling approach to support real-time structural assessment and decision-making.* To appear, *AIAA Journal.* Also AIAA-2014-1488, presented at 10th AIAA Multidisciplinary Design Optimization Conference, National Harbor, MD, January 2014, 2014.

[9] W. March, B. Xiao, and G. Biros, *ASKIT: Approximate skeletonization kernel-independent treecode in high dimensions*, SIAM Journal on Scientific Computing, (2014 (in review)).

[10] R. Palacios and C. E. Cesnik, *Cross-sectional analysis of nonhomogeneous anisotropic active slender structures*, AIAA Journal, 43 (2005), pp. 2624–2638.

[11] D. Raymer, *Aircraft Design: A Conceptual Approach*, American Institute of Aeronautics and Astronautics, 3rd ed., 1996.

[12] B. Xiao and G. Biros, *A high-dimensional kernel density estimation-based likelihood function for Bayesian image segmentation.* in review.

1.

1. Report Type

Final Report

Primary Contact E-mail

Contact email if there is a problem with the report.

kwillcox@mit.edu

Primary Contact Phone Number

Contact phone number if there is a problem with the report

617-253-3503

Organization / Institution name

MIT

Grant/Contract Title

The full title of the funded effort.

Dynamic Data Driven Methods for Self-aware Aerospace Vehicles

Grant/Contract Number

AFOSR assigned control number. It must begin with "FA9550" or "F49620" or "FA2386".

FA9550-11-1-0339

Principal Investigator Name

The full name of the principal investigator on the grant or contract.

Karen Willcox

Program Manager

The AFOSR Program Manager currently assigned to the award

Frederica Darema

Reporting Period Start Date

09/30/2011

Reporting Period End Date

01/31/2015

Abstract

This project aimed to develop novel computational statistical inference approaches for dynamic vehicle state estimation through a combination of machine learning and reduced-order modeling techniques, to develop adaptive model reduction approaches that use dynamic data to update reduced-order models for vehicle flight limit prediction, to develop approaches for online management of multifidelity models and sensor data, and to apply the new methods to quantify the benefits of a self-aware unmanned aerial vehicle (UAV) in terms of reliability, maneuverability and survivability. The project accomplished all objectives and resulted in the development of new DDDAS methodology and DDDAS algorithms, new models for a DDDAS-enabled self-aware UAV, and a demonstration of the value of DDDAS in the context of dynamic data-driven structural assessment to support decision-making for a damaged vehicle taking evasive action in a hostile environment.

Distribution Statement

This is block 12 on the SF298 form.

Distribution A - Approved for Public Release

Explanation for Distribution Statement

If this is not approved for public release, please provide a short explanation. E.g., contains proprietary information.

SF298 Form

Please attach your SF298 form. A blank SF298 can be found here. Please do not password protect or secure the PDF The maximum file size for an SF298 is 50MB.

SF298.pdf

Upload the Report Document. File must be a PDF. Please do not password protect or secure the PDF . The maximum file size for the Report Document is 50MB.

dddas-final-report.pdf

Upload a Report Document, if any. The maximum file size for the Report Document is 50MB.

Archival Publications (published) during reporting period:

D. Allaire, G. Biros, J. Chambers, O. Ghattas, D. Kordonowy and K. Willcox, Dynamic Data Driven Methods for Self-aware Aerospace Vehicles , Procedia Computer Science, Vol. 9, pp. 1206--1210, 2012

D. Allaire, G. Biros, J. Chambers, O. Ghattas, D. Kordonowy and K. Willcox, An Offline/Online DDDAS Capability for Self-Aware Aerospace Vehicles , Procedia Computer Science, Vol. 18, pp. 1959--1968, 2013

D. Allaire, D. Kordonowy, M. Lecerf, L. Mainini and K. Willcox, Multifidelity DDDAS Methods with Application to a Self-Aware Aerospace Vehicle , Procedia Computer Science, Vol. 29, pp. 1182--1192, 2014

M. Lecerf , A Data-Driven Approach to Online Flight Capability Estimation , SM Thesis, Massachusetts Institute of Technology, June 2014

L. Mainini and K. Willcox, A surrogate modeling approach to support real-time structural assessment and decision-making , accepted for publication, AIAA Journal, 2015.

D. Malhotra and G. Biros, PvFMM : A distributed memory fast multipole method for volume potentials , ACM Transactions on Mathematical Software, padas.ices.utexas.edu/static/papers/pvfmm.pdf

D. Malhotra, A. Gholami, and G. Biros, A volume integral equation S tokes solver for problems with variable coefficients , Proceedings of SC2014, IEEE/ACM, New Orleans, LA, November 2014 (Best Student Paper Finalist)

B. Peherstorfer and K. Willcox, Dynamic Data-Driven Reduced-Order Models , accepted for publication, Computer Methods in Applied Mechanics and Engineering, 2015.

B. Peherstorfer and K. Willcox, Detecting and adapting to parameter changes for reduced models of dynamic data-driven application systems , accepted for publication, Proceedings of International Conference on Computational Science (ICCS), 2015.

H. Sundar, G. Biros, C. Burstedde, J. Rudi, O. Ghattas and G. Stadler, Parallel Geometric Multigrid Methods on Unstructured Forests of Octrees , Proceedings of SC2012, IEEE/ACM, Salt Lake City, UT, November 2012

H. Sundar, D. Malhotra, and G. Biros, HykSort: a new variant of hypercube quicksort on distributed memory architectures , ACM International Conference on Supercomputing,

Eugene, Oregon, June 2013

Changes in research objectives (if any):

None

Change in AFOSR Program Manager, if any:

None

Extensions granted or milestones slipped, if any:

No cost extension granted to 1/31/2015.

AFOSR LRIR Number

LRIR Title

Reporting Period

Laboratory Task Manager

Program Officer

Research Objectives

Technical Summary

Funding Summary by Cost Category (by FY, $K)

	Starting FY	FY+1	FY+2
Salary			
Equipment/Facilities			
Supplies			
Total			

Report Document

Report Document - Text Analysis

Report Document - Text Analysis

Appendix Documents

2. Thank You

E-mail user

Apr 02, 2015 09:05:17 Success: Email Sent to: kwillcox@mit.edu